Title

Southern Ocean wind-driven entrainment enhances satellite chlorophyll-a through the summer

Journal

Journal of Geophysical Research - Oceans, 120(1)

ISSN

2169-9275

Authors

Carranza, Magdalena M

Gille, Sarah T

Publication Date

2015

DOI

10.1002/2014jc010203

Peer reviewed

AGU PUBLICATIONS

JGR

Journal of Geophysical Research: Oceans

RESEARCH ARTICLE

10.1002/2014JC010203

Southern Ocean wind-driven entrainment enhances satellite chlorophyll-a through the summer

Magdalena M. Carranza[1] and Sarah T. Gille[1]

[1]Scripps Institution of Oceanography, University of California, San Diego, La Jolla, California, USA

Key Points:
- Role of atmospheric forcing in sustaining high Chl-a in the Southern Ocean
- Wind-driven entrainment enhances satellite Chl-a in the summer
- Storm-scale Ekman pumping has little influence on satellite Chl-a in summer

Supporting Information:
- Readme
- Supporting figures
- Auxiliary materials

Correspondence to:
M. M. Carranza,
maucarranza@ucsd.edu

Citation:
Carranza, M. M., and S. T. Gille (2015), Southern Ocean wind-driven entrainment enhances satellite chlorophyll-a through the summer, *J. Geophys. Res. Oceans*, *120*, 304–323, doi:10.1002/2014JC010203.

Received 31 MAY 2014
Accepted 11 NOV 2014
Accepted article online 13 NOV 2014
Published online 23 JAN 2015

Abstract Despite being the largest High Nitrate Low Chlorophyll (HNLC) region, the Southern Ocean sustains phytoplankton blooms through the summer, when presumably there is sufficient light, but nutrients in the euphotic zone have been depleted. Physical processes that can potentially supply nutrients from subsurface waters to the euphotic zone, and promote phytoplankton growth in the summer, have not been fully explored at the large scale. By means of a correlation analysis, this study combines high-resolution satellite observations of ocean color, winds and sea surface temperature, surface heat fluxes from reanalysis and Argo mixed-layer depth (MLD) estimates to explore the role of the atmospheric forcing (i.e., winds and surface heat fluxes) on upper ocean processes that may help sustain high satellite chlorophyll-a (Chl-a) through the summer. Two physical processes that can supply nutrients to the euphotic zone are: MLD deepening, caused by wind-mixing and/or surface cooling, and Ekman pumping driven by the wind stress curl. We find that high winds correlate with high Chl-a over broad open ocean areas, suggesting that transient MLD deepening through wind-mixing (i.e., wind-driven entrainment) helps sustain high Chl-a. Wind-driven entrainment plays a dominant role on time scales associated with atmospheric synoptic storms (i.e., $<$10 days) and has a larger influence on surface Chl-a than storm scale local Ekman pumping. Based on our analysis of statistically significant correlation patterns, we identify regions in the Southern Ocean where wind-induced entrainment may play a role in sustaining summer phytoplankton blooms.

1. Introduction

The Southern Ocean plays a key role in regulating climate by sequestering atmospheric CO_2 through both the solubility and biological pumps [e.g., *Martin et al*., 1990a; *Chisholm*, 2000; *Tréguer and Pondaven*, 2001; *Marinov et al*., 2008]. It is a High Nitrate Low Chlorophyll (HNLC) region where phytoplankton abundance is primarily iron (Fe) limited [*Martin et al*., 1990b; *Boyd*, 2002; *de Baar et al*., 2005]. Although HNLC conditions abound in the Southern Ocean, phytoplankton blooms occur annually close to continental shelves and major islands, as well as in open ocean regions. Satellite observations and many studies based on in situ measurements have shown blooms that persist through the summer [e.g., *Blain et al*., 2007; *Korb et al*., 2008; *Frants et al*., 2013] (see also Figure 1a). In this work, we investigate physical mechanisms that may be responsible for sustaining phytoplankton blooms through the summer, when in most Southern Ocean locations Fe in the euphotic zone has been depleted [e.g., *Sedwick et al*., 2011; *Tagliabue et al*., 2014]. Considering that for at least 3 months of the year the HNLC Southern Ocean is not light limited [*Venables and Moore*, 2010], prolonged phytoplankton blooms likely require a continuous supply of Fe to surface waters.

Several sources of Fe to the euphotic zone have been identified in the Southern Ocean [*Boyd and Ellwood*, 2010]. These include Fe from dust deposition events, Fe that is recycled within the euphotic zone due to remineralization of organic matter, and Fe brought up to the surface from subsurface waters by means of physical processes. In seasonally ice-covered Antarctic waters, icebergs and sea-ice melting constitute an additional source of Fe [*Sedwick and Ditullio*, 1997; *Fennel et al*., 2003; *Lancelot et al*., 2009]. Phytoplankton use primarily dissolved inorganic Fe [*Sunda and Huntsman*, 1995], while dust particles are dominated by minerals of Fe [*Boyd and Ellwood*, 2010] and are not thought to be a major Fe source for most of the Southern Ocean [e.g., *Meskhidze et al*., 2007; *Wagener et al*., 2008]. Because the solubility of Fe from dust is low [*Luo et al*., 2005; *Boyd et al*., 2010; *Baker and Croot*, 2010], *Jickells* [2005] suggested there must be a large flux of particulate Fe through the deep ocean, particularly beneath the major dust plumes, that can potentially increase dissolved Fe concentrations at depth and, over the long-term can increase productivity in upwelling regions such as the Southern Ocean.

Despite abundant macronutrients such as nitrate, silicate-(Si)-depleted waters north of the Sub-Antarctic Front (SAF) can prevent growth of large phytoplankton (i.e., diatoms) and Fe-Si colimitation may occur [e.g.,

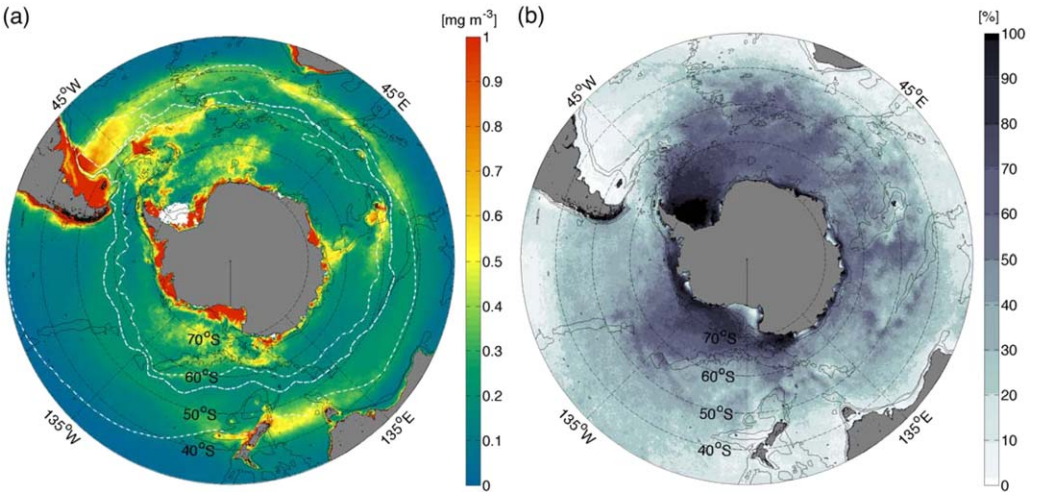

Figure 1. (a) Mean summer (DJF) Chl-a in mg m^{-3} based on 12 years of satellite Chl-a data (2000–2011). The mean positions of the Sub-Tropical (STF), Sub-Antarctic (SAF), and Polar Fronts (PF, from north to south) are shown with dashed white contours [from *Orsi et al.*, 1995]. (b) Percentage of weeks with missing values in summer Chl-a data due to cloud and ice coverage, sun glint, and low sun angles. Thin black lines show the bathymetric contours of 1000 and 3000 m.

Hoffmann et al., 2008; *Martin et al.*, 2013]. In the summertime, even nitrate may become depleted, especially to the north of the Sub-Tropical Front (STF) [*Pollard et al.*, 2002]. Hereafter, we will use the word nutrients when referring to the limiting nutrient, which based on observations could potentially be Fe, Si, or nitrate depending on the region.

Nutrient supply in the Southern Ocean is thought to be controlled by ocean dynamics [e.g., *de Baar et al.*, 1995; *Hense et al.*, 2003; *Fennel et al.*, 2003; *Moore*, 2004; *Meskhidze et al.*, 2007]. Physical processes such as mixing, upwelling, horizontal advection, secondary circulation associated with mesoscale features (i.e., eddies and fronts), and entrainment due to changes in the mixed-layer depth (MLD), all can contribute to the supply of nutrients to the euphotic zone. In this study, we focus on physical processes controlling the vertical exchange of nutrients from subsurface reservoirs to the euphotic zone through MLD dynamics.

The MLD controls nutrient availability as well as phytoplankton exposure to light and thus is of great relevance for phytoplankton growth [e.g., *Sverdrup*, 1953; *Mitchell and Holm-Hansen*, 1991]. The level of mixing and turbulence in the upper ocean can also influence grazing rates [*Behrenfeld*, 2010] and has consequences for the redistribution and accumulation of phytoplankton itself within the mixed layer, which may lead to surface blooms regardless of the depth of the mixed layer [*Taylor and Ferrari*, 2011a]. Despite the recent debate on the extent to which the MLD is relevant for phytoplankton bloom development [*Behrenfeld*, 2010; *Taylor and Ferrari*, 2011a; *Chiswell*, 2011], the atmospheric forcing that sets up stratification and mixing in the upper ocean on time scales relevant to phytoplankton growth and accumulation (days to weeks) likely impacts surface phytoplankton blooms.

On time scales of days to weeks, the MLD is largely determined by the turbulent mixing caused by the winds, and buoyancy forcing. Entrainment of nutrient-rich and submixed-layer waters, which are typically cold, occurs when the mixed layer deepens. Numerical models and observational evidence show that wind-induced mixing events accompanied by deepening, and/or erosion of the seasonal thermocline can significantly increase nutrient concentrations in the euphotic zone [*Klein and Coste*, 1984; *Eppley and Renger*, 1988; *Marra et al.*, 1990; *Lévy et al.*, 2009]. Nutrient entrainment to the mixed layer follows the wind action with a time lag of hours, which decreases with stronger winds [*Klein and Coste*, 1984], and because phytoplankton populations can double more than once per day, and phytoplankton grazers are capable of population increases at much higher rates (i.e., up to five doublings per day [e.g., *Miller et al.*, 1991; *de Baar et al.*, 2005]), the response of phytoplankton is expected to be concomitant with wind-driven entrainment at daily scales. In extratropical latitudes, modeling studies show that changes in the MLD and the heat flux through the base of the mixed layer play an important role in the development of sea surface temperature (SST) anomalies in the summer, when the entrainment rate is generally dominated by wind-induced mixing [*Alexander et al.*, 2000]. In addition, the wind stress curl drives vertical velocities via Ekman pumping and can modulate the entrainment process [e.g., *McPhaden et al.*, 2008].

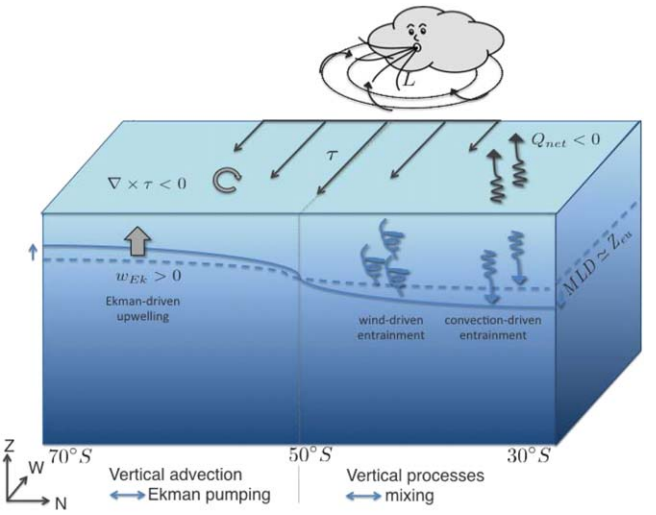

Figure 2. Schematic of physical processes considered in this study that can lead to entrainment of nutrient-rich and typically cold subsurface waters into the euphotic zone. MLD: mixed layer depth, Z_{eu}: euphotic depth, τ: wind stress, Q_{net}: net heat fluxes, and w_{Ek}: Ekman pumping.

Global studies have shown that winds have a measurable influence on satellite chlorophyll-a (Chl-a) variability [*Kahru et al.*, 2010]. In most parts of the global ocean, high wind speeds correlate with high Chl-a, implying either that winds deepen the mixed layer resulting in more nutrients being entrained into the upper ocean promoting phytoplankton growth, or alternatively that winds mix the deep Chl-a maximum up to the surface. This is not the case in the Southern Ocean where wind speed and Chl-a tend to be negatively correlated on monthly to seasonal time scales [*Fitch and Moore*, 2007; *Kahru et al.*, 2010]. The most plausible explanation for the inverse relationship is that in regions with very deep mixed layers in late winter, strong winds tend to deepen the mixed layer enough to remove phytoplankton from the euphotic zone and thus reduce their mean light levels, impacting their growth rates. Although the MLD is shallowest in the summer, the water just below the seasonal mixed layer has potentially low stratification, and small anomalous increases in summer winds can therefore easily remix the upper layer, reestablishing deep mixed layers, which would tend to decrease Chl-a [*Kahru et al.*, 2010]. The suggested inverse relationship between Chl-a and MLD is in agreement with the relationship observed between Fe-addition experiments [*de Baar et al.*, 2005], where those in the Southern Ocean associated with deeper mixed layers showed lower surface Chl-a values.

The Southern Ocean is exposed to strong surface winds associated with the high atmospheric synoptic activity that characterizes the Southern Hemisphere all year round [*Hoskins and Hodges*, 2005]. The Southern Annular Mode (SAM) has intensified in response to Antarctic ozone depletion, leading to stronger surface westerlies, particularly during austral summer [*Thompson et al.*, 2011], when coincidentally phytoplankton blooms tend to peak. Because the deepening of the MLD has the potential to entrain nutrients and promote phytoplankton growth when light is not limiting, the MLD may play a critical role in the summer if wind-induced mixing events are strong enough to deepen the mixed layer. We will show that, despite strong summer winds, summer MLDs do not vary substantially from the seasonal mean. They are shallower and closer to the euphotic depth, potentially allowing for anomalous deepening of the seasonal MLD to entrain nutrients efficiently [e.g., *Fauchereau et al.*, 2011].

The purpose of this study is to explore the influence of atmospheric synoptic storms on summer phytoplankton abundance in the Southern Ocean. We focus on the roles of winds and buoyancy forcing, which can deepen the mixed layer resulting in entrainment from below the base of the mixed layer. We also explore the contribution of Ekman-induced upwelling to the entrainment process. A schematic of the physical processes considered is shown in Figure 2. Our approach is a correlation analysis that combines data drawn from a broad range of sources including satellite data, reanalysis and Argo floats. We correlate high-resolution physical variables that can elucidate the dynamics of the MLD with satellite Chl-a, which serves as a proxy for phytoplankton biomass. Because over coastal areas and close to islands/plateaus along the Antarctic Circumpolar Current (ACC) pathways the dynamics are expected to be influenced by other processes that are not necessarily wind related, we focus our analysis on open ocean phytoplankton blooms. Based on our analysis of statistically significant correlation patterns, we identify regions in the Southern Ocean where wind-induced entrainment may play a role in sustaining summer blooms.

2. Data and Methods

The entrainment rate of any given property at the base of the mixed layer, *h*, can be written as [e.g., *de Szoeke*, 1980; *Musgrave et al.*, 1988; *Close and Goosse*, 2013]:

$$w_e = \frac{\partial h}{\partial t} + w_{Ek}(h), \quad (1)$$

where the first term in the right-hand side represents turbulent entrainment as the MLD deepens, and the second term is a modulation of entrainment caused by nonturbulent vertical advection due to Ekman pumping (w_{Ek}). Deepening of the MLD can be caused by wind-induced mixing and/or surface cooling, two processes that can generate turbulence at the base of the mixed layer. On the other hand, w_{Ek} represents the vertical displacement of the material surface that defines the base of the mixed layer, solely as a result of mixed-layer divergences driven by wind stress curl ($w_{Ek} = \nabla \times \tau / \rho f$). In the Southern Hemisphere where $f < 0$, Ekman-induced upwelling (i.e., Ekman suction, $w_{Ek} > 0$) occurs when the wind stress curl is negative. Both contributions to the entrainment rate are tightly linked to the atmospheric forcing, for which satellite and reanalysis data are available, allowing us to address the potential impact of these processes in a large-scale context.

2.1. Satellite Data

At least, weekly temporal sampling is needed in order to capture variability driven by fast-moving atmospheric storm systems and phytoplankton turnover. Here we use 9 years of daily and weekly (i.e., 8 days) satellite estimates of Chl-a, SST, and winds for the period June 2002 to May 2011 when all observations are available. The start and end of this period are dictated by the Advanced Microwave Scanning Radiometer (AMSR-E), which is used for SST. In our analysis, we only include data from the austral summer months (December, January, and February, DJF) that comprise a total of 812 days.

Chl-a is used as a proxy for phytoplankton biomass. Although in some regions of the world's oceans Chl-a may respond more closely to physiological changes rather than phytoplankton biomass, in the Southern Ocean, Chl-a and phytoplankton carbon are well correlated [*Le Quéré et al*., 2002; *Behrenfeld et al*., 2005; *Arrigo et al*., 2008]. We use Chl-a data from multiple sensors merged by the European Space Agency's GlobColour project. The data are reported on a 25 km × 25 km grid, and are determined using the bio-optical model described by *Maritorena and Siegel* [2005]. The main advantage of using the merged product is the increased number of observations in the Southern Ocean, where persistent cloud coverage represents an obstacle for ocean color sensors. Cloudiness shows a pronounced seasonal cycle over the Southern Ocean with higher cloud incidence during the winter season [*Verlinden et al*., 2011], when Chl-a values are presumably low. In addition to clouds, ice cover and low sun angles south of 65°S often result in no valid data, and more than half of the year Chl-a cannot be retrieved. However, in the summer, the percentage of missing data is significantly reduced, and only regions close to the Antarctic continent are severely impacted by missing data (Figure 1b).

A phytoplankton bloom is generally defined as an increase in Chl-a concentration relative to a threshold value [e.g., *Henson and Thomas*, 2007; *Fitch and Moore*, 2007; *Racault et al*., 2012]. *Behrenfeld* [2010] suggests looking at changes in net population growth rates (i.e., $r = \ln(\text{Chl-a}_{t1}/\text{Chl-a}_{t0})/\Delta t$) rather than biomass (i.e., Chl-a). In the Southern Ocean, the use of net phytoplankton growth rates significantly limits the number of observations, even when considering 4 day averages to compute initial and final Chl-a values for a given week. Here we are interested in intraseasonal variability and use Chl-a anomalies relative to a climatological mean to preserve the highest possible temporal resolution. We find that the absolute value criterion (e.g., Chl-a > 0.8 mg m^{-3} in *Fitch and Moore* [2007]) misses small-amplitude phytoplankton blooms, and for this study we consider positive Chl-a anomalies to be indicative of a bloom. The criterion we use captures more open ocean blooms, where winds and the dynamics of the mixed layer are likely to play a major role in sustaining high Chl-a.

Chl-a anomaly maps were computed for each day and week using the ratio of observed Chl-a to a multiyear time mean and expressed as a percentage, i.e.:

$$\text{Chl-a}' = \frac{\ln(\text{Chl-a}) - \overline{\ln(\text{Chl-a})}}{\overline{\ln(\text{Chl-a})}} \times 100. \quad (2)$$

Since Chl-a is approximately log-normally distributed, we use a geometric mean (i.e., $\overline{\text{Chl-a}} = \exp(\overline{\ln(\text{Chl-a})})$ to compute mean values whenever necessary. The use of the log-normal distribution as a model for the variability of Chl-a has been supported both empirically and theoretically [*Campbell*, 1995]. This assumption works well if the variance is relatively low [*IOCCG*, 2004]. However, in many cases, Chl-a binned data show a bimodal structure. We find that our results are not sensitive to the way in which Chl-a anomalies were calculated, and the quantity Chl-a $-\overline{\text{Chl-a}}$ yields similar correlation patterns.

In the range of Chl-a values typical for the Southern Ocean (0.2–2 mg m^{-3}), satellite Chl-a algorithms tend to underestimate Chl-a by a factor of 2–3 compared to in situ measurements [*Kahru and Mitchell*, 2010; *Guinet et al*., 2013]. Surface Chl-a may also underestimate vertically integrated values of Chl-a for the euphotic zone due to subsurface maxima [*Holm-Hansen et al*., 2005; *Knox*, 2007; *Arrigo et al*., 2008]. Assuming an absolute bias offset that is uniform across the Southern Ocean, systematic underestimation of Chl-a will not impact our results, since the analysis of correlation patterns is based on anomalies.

We use the Cross-Calibrated Multi Platform (CCMP) ocean surface winds. These winds are produced using a variational analysis method that blends data from multiple satellites [*Atlas et al*., 2011]. CCMP winds are available on 25 km × 25 km grids and are distributed by the Physical Oceanography Distributed Active Archive Center (PO.DAAC). By taking advantage of the differences in the orbits between the platforms and sampling times, they provide reliable wind fields at 6 h temporal resolution. In comparison with observations from the Stratus buoy (20°S, 85°W), CCMP winds provided higher coherence at high frequencies than single satellite observations for QuikSCAT, WindSat, or ASCAT winds. CCMP winds yielded higher correlations with MLD than did other wind products, and in this paper, only results from CCMP winds are presented.

To compute w_{Ek}, wind stress was estimated following *Risien and Chelton* [2008] from the meridional and zonal components of the wind. Wind stress curl fields were computed using spherical coordinates and smoothed using a moving block average with a flat kernel of 4 × 6 grid cells, resulting in an effective resolution of 100 km × 150 km (results were not sensitive to the choice of boxcar versus circular or Gaussian filter).

We use microwave SSTs from the AMSR-E instrument carried on board the Aqua satellite. These data are provided by Remote Sensing Systems (RSS) on a 25 km × 25 km grid (version 7). Microwave SSTs are not strongly affected by clouds, in contrast with infrared SSTs or ocean color, both of which provide gappy data in the Southern Ocean due to persistent cloud cover. Missing data in AMSR-E SST are due to high wind speed (>20 m s^{-1}), sun glint, rain, sea ice, or proximity to land. The AMSR-E measurements tend to overestimate SST due to undetected ice, and in summer they have been shown to be warmer than in situ observations [*Dong et al*., 2006], whereas infrared SSTs tend to underestimate surface temperature due to cloud contamination. For completeness, we also tested daytime infrared SSTs from the Moderate Resolution Imaging Spectroradiometer (MODIS-T on Terra). MODIS-T SSTs yield similar results in correlation coefficients between the variables, albeit with larger statistical uncertainties because of data dropouts due to cloud cover.

2.2. Reanalysis Data

For surface heat fluxes, we use the coupled global NCEP Climate Forecast System Reanalysis (NCEP/CFSR) [*Saha et al*., 2010a]. This reanalysis provides higher resolution (1 h and 0.5° × 0.5°) compared with previous reanalysis. Since NCEP/CFSR reanalysis incorporates satellite measurements, especially in the Southern Hemisphere, the accuracy increases over time [*Saha et al*., 2010b], and the net ocean surface heat flux (Q_{net}) has smaller biases than the NCEP/NCAR reanalysis [*Xue et al*., 2011]. Here positive Q_{net} is defined as flux into the ocean (i.e., the ocean heats). Although CFSR reanalyses show significant improvements over previous reanalyses [*Xue et al*., 2011], remaining uncertainties in the surface heat fluxes could impact our results. To gain confidence in our results, we repeated the analyses using the ERA-Interim heat fluxes from the European Centre for Medium-Range Weather Forecasts (ECMWF), and overall results did not change.

2.3. Argo Mixed-Layer Depth

Most large-scale studies that address physical mechanisms responsible for the observed patterns in satellite Chl-a rely on numerical models or ocean reanalysis when considering the effect of stratification and MLD dynamics [e.g., *Llido et al*., 2005; *Alexander et al*., 2008; *Behrenfeld*, 2010; *Fauchereau et al*., 2011]. Here we use in situ MLD estimates for 48,588 summer Argo profiles in the Southern Ocean during the period 2001–2011 [*Holte et al*., 2010]. The number of Argo profiles increased substantially over time (from 35 in 2001 to >1807 in 2004, and >7974 in 2011). *Holte and Talley* [2009] provided five MLD estimates. In summer, differences between these are typically less than 10 m [*Dong et al*., 2008; *Stephenson et al*., 2012], and all definitions of the MLD produced similar patterns when correlated with other variables. Here we show results based on the density threshold criterion of 0.03 kg m^{-3} [*de Boyer Montégut et al*., 2004]. In winter months, *Stephenson et al*. [2012] showed ocean heat content to provide a better measure of upper ocean variability than MLD, but for this summer-oriented study we focus on MLD, since MLD can influence nutrient availability in the euphotic zone.

2.4. Statistical Analysis

To explore the influence of atmospheric storms on upper ocean physics and summer Chl-a variability, we compute maps of local correlation coefficients between anomalies of Chl-a and physical variables: wind speed, Q_{net}, w_{Ek}, and SST. At each grid cell, a time series of anomalies of each of these variables was constructed (except for w_{Ek}), from which local correlation coefficients were computed.

To match the spatial resolution of all data sets, we have chosen to coarsen the resolution of Chl-a, SST and winds to match that of surface heat fluxes by bin averaging into a $0.5^\circ \times 0.5^\circ$ grid.

Because MLD deepening due to turbulent processes and Ekman-induced upwelling may be expected to operate on different time scales [*de Szoeke*, 1980], we tested both daily and weekly correlations. For most of the analysis shown, we use daily anomalies calculated by subtracting monthly climatological means in order to eliminate the seasonal variability and long-term trends. When using weekly anomalies, we removed the multiyear weekly means.

Consecutive data dependence of daily data can reduce the number of degrees of freedom and impact the evaluation of statistical significance. To make significance more robust when testing for daily correlations, we high-pass filtered the data in time using a cutoff frequency of 10 days chosen to highlight the effects of synoptic storm systems [*Vera*, 2003]. Missing data in daily fields were linearly interpolated in time prior to filtering and subsequently padded as missing values. For daily correlations, we show results obtained by subtracting from the original time series of anomalies the low-pass filtered time series using an 11 point moving average run forward and backward to preserve the phase (i.e., a 21 point triangular filter). Other filters commonly used to extract the variability associated with the atmospheric synoptic scale were also tested (e.g., a Butterworth four-pole filter following *Nakamura et al*. [2002]) and gave qualitatively similar results.

The SAM and El Niño Southern Oscillation (ENSO) are the dominant modes of climate variability in the Southern Ocean, and both can influence upper ocean dynamics and Chl-a [e.g., *Le Quéré et al*., 2002; *Lovenduski and Gruber*, 2005; *Sallée et al*., 2010]. Here we are interested in the response of Chl-a to local wind forcing, and we high-pass filter the data in the time domain to minimize the impact of low-frequency or remote coupled ocean-atmospheric forcings. High-frequency variability associated with the SAM [e.g., *Baldwin*, 2001] may remain in high-pass filtered time series. Our results, however, are largely unchanged if we specifically remove the variability associated with SAM and ENSO from all anomaly time series by subtracting the least squares regression onto SAM and ENSO indices.

Oceanic mesoscale features can significantly modify upper ocean physics and biology and are marginally resolved at 25 km resolution. Consistent with the first baroclinic Rossby deformation radius, satellite Chl-a shows mesoscale structures smaller than 175 km south of 30°S that are comparable to decorrelation scales of altimetry and SST data [*Krauss et al*., 1990; *Stammer*, 1998; *Doney*, 2003]. The anisotropy found in altimeter data is, however, less apparent in Chl-a mesoscale variability [*Doney*, 2003]. To suppress oceanic mesoscale processes in our data, we spatially smooth anomaly fields of all variables using a rectangular window of 14×14 grid points (350 km $\times$ 350 km). For Chl-a, we smoothed $\ln(\text{Chl-a})$ and the geometric means prior to computing anomalies to avoid unrealistic large values. Given that mean currents in the ACC are roughly 20 cm s^{-1} (or 17 km d^{-1}), at daily scales and 175 km effective resolution advection can be neglected, and the correlation patterns reflect local processes.

When testing for a dependence relation between the variables, we use the nonparametric Spearman correlation coefficient [*Gibbons*, 1985] because it does not assume prior knowledge of the probability distribution function to determine statistical significance and it is less sensitive to outliers. Spearman's test has difficulties when the sample size is very small and therefore we compute correlations only when $N > 10$.

SST is often used as a proxy for nutrients with the implicit assumption that SST variability is associated with upwelling or entrainment. However, there are multiple feedbacks between the oceanic and atmospheric boundary layers through changes in surface heat fluxes that can impact the SST and other physical variables. To avoid spurious correlations, for parts of this study we compute partial correlations [see, e.g., *Box et al*., 1994]. Partial correlations measure the degree of association between two variables with the effect of a controlling variable removed. The method essentially involves a correlation between the residuals that result from the linear regression of each variable against the controlling variable.

In this study, we are mostly interested in the sign of correlations and the processes that may be driving the observed patterns. The magnitude of a change in SST that is expected given an increase in winds may be

useful, for instance, for the design of observational experiments at sea. In the supporting information, we also supply slopes of the linear regression model for all significant correlations presented here.

To address how much of the summer MLD variability observed in Argo is accounted for by surface forcing, we correlate anomalies of the MLD with anomalies of wind speed, Q_{net} and SST. For each profile, MLD anomalies were computed relative to a summertime mean MLD field (Figure 4a), constructed by averaging Argo MLD estimates onto a $2^\circ \times 4^\circ$ grid for the summer season. The number of Argo estimates averaged in each bin is shown in Figure 4c. Climatological monthly MLDs were also considered but these resulted in significant data loss due to the poorer coverage in monthly mean MLD maps. To correlate MLD anomalies with satellite variables, we found the closest observations of the physical variables in space and time that matched with the location and time of the Argo profiles in $2^\circ \times 4^\circ$ bins, and within a time window of 3 days. Because time series of data pairs in each bin are constrained by the availability of Argo profiles and, therefore, very gappy, we chose not to spatially smooth or high-pass filter the data in time when correlating against MLD. However, a correlation test using filtered satellite and reanalysis fields against unfiltered MLD anomalies yields similar results.

3. Results

3.1. Southern Ocean Phytoplankton Blooms

Mean summer Chl-a based on 12 years of ocean color data is shown in Figure 1. Large values in Chl-a are found over most of the continental shelves (>1 mg m^{-3}, e.g., around South America and the Antarctic continent), downstream of Drake Passage, and near major islands (e.g., Kerguelen Plateau, South Georgia and South Sandwich Islands, Crozet Islands), but also relatively large values (>0.4 mg m^{-3}) are observed in open ocean areas sometimes associated with the mean position of frontal features (e.g., in the STF, over the western part of ocean basins, along the northern most dashed white line in Figure 1a). These areas of high Chl-a coincide with areas of elevated surface particulate organic carbon and primary production in the Southern Ocean [*Moore and Abbott*, 2000; *Sokolov and Rintoul*, 2007; *Arrigo et al*., 2008; *Allison et al*., 2010]. The asymmetry in Chl-a along the 40°S–50°S band between the Atlantic-Indian sector and the eastern Pacific was noted by *Thomalla et al*. [2011], who attributed the lower Chl-a values in the Pacific to limited Fe supply from the deep due to relatively shallower winter mixed layers.

Although bloom initiation in the Southern Ocean south of ~40°S occurs in the spring (September–November) [*Thomalla et al*., 2011], elevated values of Chl-a can persist for more than 12 weeks [*Racault et al*., 2012]. In Figure 3, we show the month of occurrence of maximum Chl-a based on the climatological annual cycle (i.e., averaged monthly mean maps of Chl-a). We also calculated the most frequent month of occurrence of the peak by keeping track of the month of maximum for each year in the record and computing the mode, and a similar structure was obtained. Chl-a tends to peak in the summer over large areas (red tones in Figure 3) within the ACC, whereas to the north of the ACC Chl-a tends to peak in the spring (blues in Figure 3). To the north of the STF, Chl-a reaches its maximum in winter (dark greens in Figure 3) when the MLD is deepest (70–100 m in the Atlantic and Pacific and somewhat shallower in the subtropical Indian sector), and its minimum in the summer when the MLD is shallowest (~40 m, see Figure 4a). This agrees with the findings of *Thomalla et al*. [2011], who carried out a detailed analysis of the seasonal cycle of Chl-a in the Southern Ocean, showing that the bloom initiation progresses meridionally with the latitudinal progression in light intensity [*Racault et al*., 2012].

Regional differences in the phasing of the seasonal cycle suggest nutrient limitation may be more pronounced during different times of the year depending on the location. Thus, the summer season based on the calendar year may not resemble a nutrient-limited regime everywhere in our domain. For example, north of the STF where Chl-a reaches its maximum in late winter, a nutrient-limited regime will likely be more pronounced in the spring. As an alternative to the DJF definition of summer, we also considered the 2 months that follow the month of the Chl-a peak in the annual cycle for our analysis, defining a summer-like season for each grid cell that best represents the time of the year when phytoplankton growth is presumably nutrient limited. Correlations based on the summer-like season give slightly larger values north of the STF, but overall patterns remain unchanged and, throughout this paper results we show are for the austral summer months (DJF).

3.2. Summer Atmospheric Forcing and MLD Variability

In this section, we examine the impact of atmospheric forcing (i.e., winds and surface heat fluxes) on summertime MLD dynamics, since this is a key step to evaluate how anomalies in Chl-a are related to physical forcing.

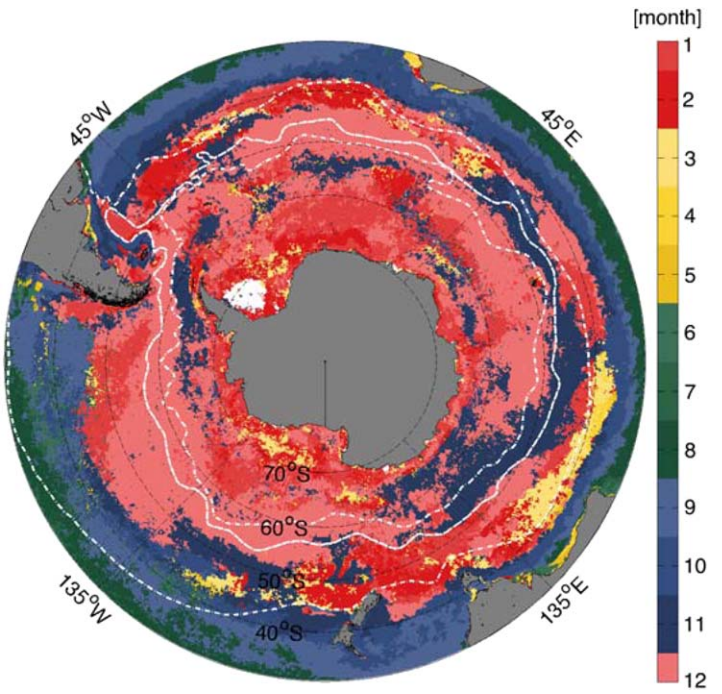

Figure 3. Month of maximum Chl-a, based on 12 years of monthly data (2000–2011). The mean positions of the STF, SAF, and PF (from north to south) are shown with white contours [from *Orsi et al.*, 1995].

Winds over the Southern Ocean are strong year round, with little seasonal variation [*Yuan*, 2004; *Gille*, 2005]. Mean summer winds are $\sim$12 m s^{-1} in the circumpolar band (Figure 5a), but extremes are much greater. Weekly and daily anomalies can reach up to 10 and 20 m s^{-1}, respectively. In regions where the winds are weaker (i.e., in the subtropical and polar bands), there is considerable gustiness (not shown), and ocean circulation models show the Southern Ocean MLD to be sensitive to gustiness in the winds [*Lee et al.*, 2008].

The MLD is shallowest in the summer (MLD $<$ 90 m, see Figure 4a) and closer to the euphotic depth ($\sim$100 m in oceanic waters surrounding Antarctica) [*Knox*, 2007], which allows for optimal conditions of light for phytoplankton to grow. As the MLD shallows, strong wind events are more effective in deepening the mixed layer to entrain water from just below the base of the mixed layer. The summer MLD varies substantially in the Southern Ocean (Figure 4b) with a standard deviation ranging from 15 to 30 m. Variability is highest in regions with deep seasonal mixed layers (Figure 4a). However, Argo data do not show extremely deep summer MLDs. This suggests that in the summer, strong wind events may reduce upper ocean stratification without completely eroding the seasonal mixed layer.

By enhancing vertical mixing in the upper ocean, strong winds have the potential to entrain cold waters into the mixed layer thus influencing the mixed-layer heat budget [*Bonekamp et al.*, 1999] and producing cold SSTs. This would imply a negative correlation between wind speed and SST anomalies, as discussed by *Price* [1981] for hurricane conditions. However, SST can also induce changes in the winds by setting up instabilities in the marine atmospheric boundary layer [*Wallace et al.*, 1989] with implications for surface heat fluxes. In the extratropics, *Xie* [2004] interpreted negative correlations between wind speed and SST as indicating that the ocean passively responds to wind-induced latent and sensible heat fluxes. In our analysis, wind speed and SST are also strongly correlated with Q_{net} (not shown). To suppress the effect of surface heat fluxes, in Figure 5b, we show partial correlations between wind speed and SST controlling for Q_{net}. Statistically significant negative correlations arise over the entire domain, and suggest that SST changes in response to entrainment of subsurface waters. Our correlations indicate wind speed alone can explain as much as 80% of the variance observed in SST.

MLD data from Argo are less numerous than SST or wind data, but they support the hypothesis inferred from the SST versus wind correlation, that strong summer wind events lead to cooler SSTs, because they deepen the mixed layer. Figure 6a shows positive correlations between wind speed and MLD throughout the Southern Ocean, implying high winds deepen the mixed layer. To a lesser extent, surface cooling also contributes to deepening the MLD (i.e., negative correlations between Q_{net} and MLD in Figure 6b). On average, wind speed explains 21.8% of the MLD variance versus 16.7% explained by Q_{net}. The lower number of statistically significant correlations in Figure 6b compared to Figure 6a also suggests that in the summer winds have greater influence on MLD than Q_{net}. Correspondingly Figure 6c indicates that deep mixed layers are correlated with cold SSTs, supporting the hypothesis that anomalous deep mixed layers permit entrainment of cold water into the mixed layer. Changes in the MLD account for roughly 30% of the SST variance, and therefore SST alone may not be a good proxy for MLD. To suppress feedbacks with the marine atmospheric boundary

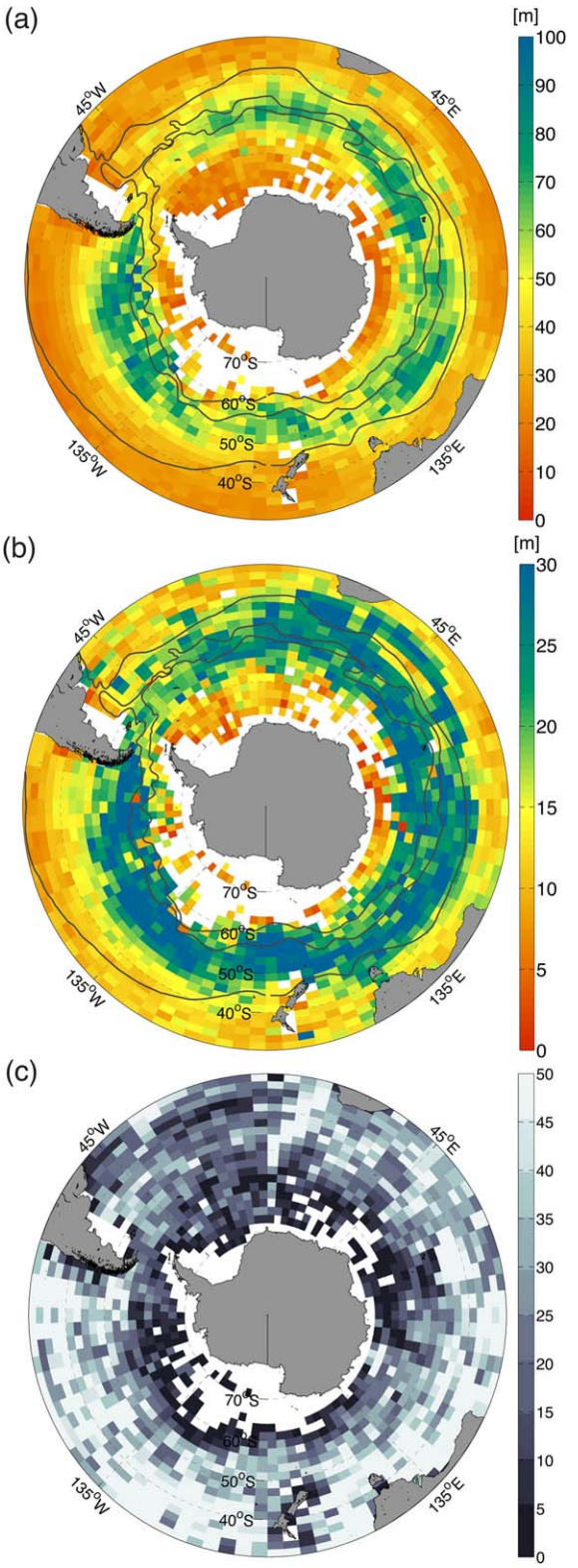

Figure 4. (a) Mean summer (DJF) MLD and (b) standard deviation of the summer MLD averaged in 2° × 4° bins for the period 2001–2011. The MLD is defined using a density threshold criteria (threshold of 0.03 kg m^{-3}, following *de Boyer Montégut et al.* [2004]). (c) Number of summer (DJF) Argo MLD estimates averaged in each bin. The mean positions of the STF, SAF, and PF (from north to south) are shown with black contours [from *Orsi et al.*, 1995].

layer, partial correlation coefficients were also computed. These patterns, based on fewer data points constrained by the availability of three variables, showed fewer bins with statistically significant correlations (not shown) but larger correlation coefficients of the same sign as shown in Figure 6. Nonsignificant correlations to the south of the ACC in Figure 6 may reflect both salinity effects that are important due to ice melting in the summer and the scarcity of Argo profiles. Correlations also tend to be nonsignificant over the Atlantic sector, where the number of available MLD estimates is smaller than in the Pacific (Figure 4c).

To summarize, the results in Figure 6 imply that wind speed contributes more than Q_{net} to summer MLD variability, but both variables influence stratification and contribute to MLD variance and are thus hypothesized to influence Chl-a.

3.3. Effect of MLD Deepening on Chl-a

In this section, we evaluate how stratification and upper ocean mixing (caused by winds and surface heat fluxes) exert a control on Chl-a variability. If MLD deepening delivers nutrients into the seasonal mixed layer, we expect positive correlations between Chl-a and wind speed anomalies (i.e., wind-driven entrainment) and negative correlations between Chl-a and Q_{net} (i.e., convection-driven entrainment).

To investigate the influence of wind-driven entrainment on Chl-a, we mapped local correlation coefficients between anomalies of Chl-a and wind speed (Figure 7a). Because the atmospheric synoptic scale associated with storm systems exhibits fluctuations with periods of less than 10 days [*Vera*, 2003], here we use daily anomalies. Compared with weekly data, daily data, although sparser in space and time, yield larger areas with significant

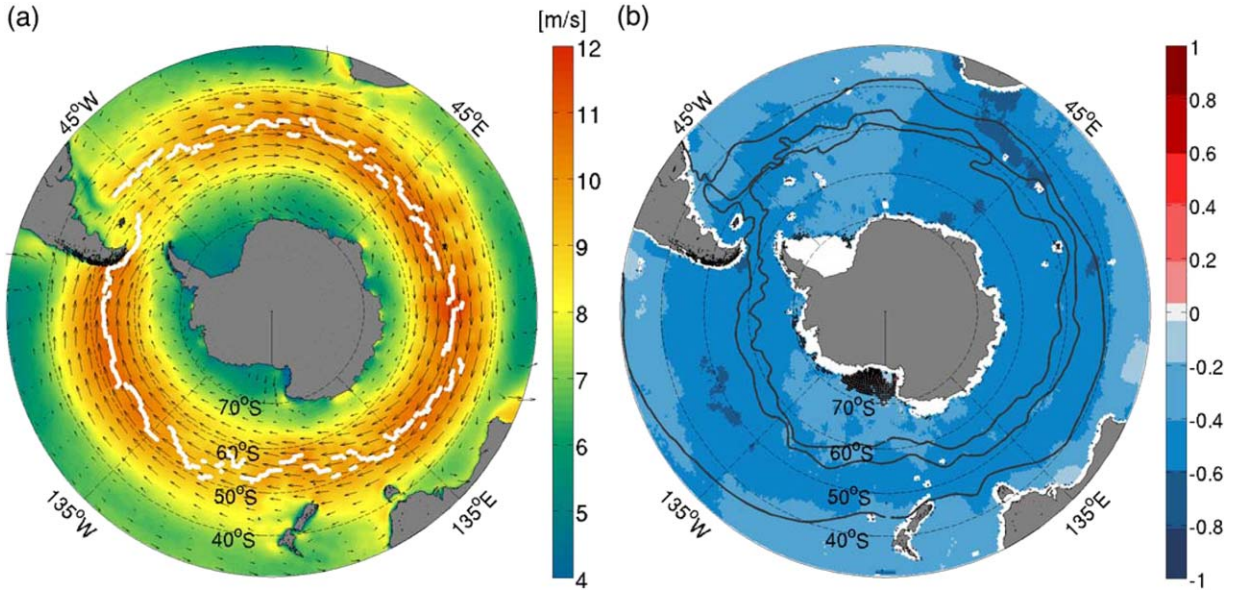

Figure 5. (a) Mean summer (DJF) winds in m s^{-1} based on 12 years of CCMP wind data (2000–2011). The white dotted contour indicates the mean position of the maximum westerlies. (b) Partial correlation coefficients between daily anomalies of wind speed and SST after removing the effect of Q_{net} for summer data of 2002–2011. Anomalies were spatially smoothed and high-pass filtered in the time domain to highlight the effect of atmospheric synoptic storms (i.e., spatial scales >350 km and time scales <10 days). Dotted areas indicate the correlation is not significant at the 90% level. The mean positions of the STF, SAF, and PF are shown in black contours.

correlations between Chl-a and wind speed. Moreover, the direct relationship between wind speed and Chl-a prevails when high-pass filtering daily data in the time domain (see section 2.4), and these are the results we show in Figure 7. Even though winds may be influenced by surface heat fluxes (e.g., through enhanced turbulence in the atmospheric boundary layer), we do not show partial correlations in Figure 7, because we are not interested in identifying, for example, whether the high wind correlation is related to surface heat fluxes. Nonetheless, we tested partial correlations in all cases, and the results did not change significantly.

In contrast with the findings of *Kahru et al*. [2010] who used year-round data, in the summer strong wind events show a positive influence on Chl-a over large areas (Figure 7a). Even over regions where we find the deepest mixed layers (e.g., the southeast Pacific, see Figure 4a), strong winds correlate with high Chl-a (Figure 7a). This may imply summer storms are effective in breaking down stratification enough to entrain nutrients, without completely eroding the seasonal MLD, which would expose phytoplankton to light limitation stress. In particular, the regions to the north of the STF, the eastern Pacific including the region between the PF and SAF west of Drake Passage, and upstream of Kerguelen Plateau show significant positive correlations between wind speed and Chl-a (Figure 7a) that persist on weekly time scales (not shown).

One might hypothesize that Fe-rich dust could be deposited by high wind events, and subsequently dissolve to initiate a bloom leading to positive correlations between wind speed and Chl-a. However, our results indicate no correlation between wind speed and Chl-a at 1 week time lags (not shown), even when we smooth spatially (with a spatial filter of 1 × 5 grid cells given the ACC moves at ~125 km $week^{-1}$) to account for advection, implying no clear connection with dust deposition. Further tests of lagged correlations between wind speed and Chl-a using daily data show that the correlation is significant at zero and 1 day lags but mostly vanishes after 2 days. The time response of Chl-a to high winds is more consistent with nutrient supply due to wind-driven entrainment at the base of the mixed layer than with direct dust deposition. Although dust may not be immediately bioavailable, it is nevertheless presumably a source of Fe to the deep ocean [*Jickells*, 2005].

Although entrainment due to MLD deepening may play an important role in the open ocean, as suggested from correlations in section 3.2, regions where the correlation between wind speed and Chl-a is not statistically significant (Figure 7a) may indicate that bioavailable Fe is supplied by means other than entrainment due to MLD deepening, or that the waters brought up lack bioavailable Fe (e.g., where waters have not recently interacted with the oceanic seafloor to pick up Fe and/or are distant from dust sources.)

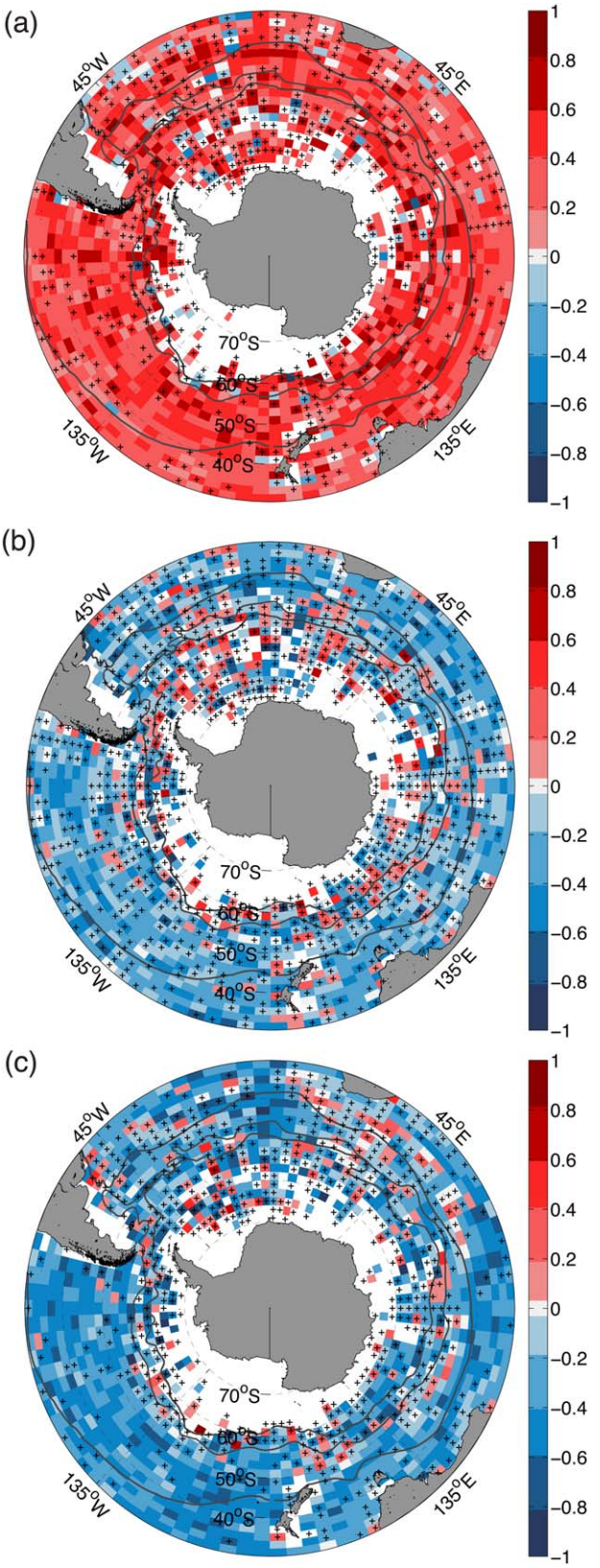

Figure 6. Local summer (DJF) correlation coefficients between daily anomalies of (a) wind speed and MLD, (b) Q_{net} and MLD, and (c) SST and MLD. Because MLD data are sparse, here we do not smooth out or filter the data in time. Cross-hatched areas indicate r is not significant at the 90% level. The mean positions of the STF, SAF, and PF are shown in black contours.

Surface cooling might be predicted to deepen the MLD (Figure 6b) and increase Chl-a. Significant negative correlations between anomalies of Q_{net} and Chl-a indicate surface cooling has an impact on Chl-a to the north of the STF (Figure 7b), potentially through MLD deepening. However, low and mostly nonsignificant correlations in Figure 7b demonstrate this is not a dominant mechanism that drives Chl-a variability in the summer over most of the ACC. This result underscores the importance of wind-induced entrainment in sustaining summer phytoplankton blooms.

3.4. Effect of Ekman Pumping on Chl-a

In addition to deepening the MLD, the wind can also drive Ekman-induced upwelling associated with the wind stress curl. The mean curl of the wind stress is expected to be positive in the subtropical band up to the latitude where the westerlies reach their maximum (~50°S, white dotted line in Figure 8), and negative toward the south up to the maximum in the polar easterlies. In the Southern Hemisphere, the mean wind stress curl translates into upwelling over most of the ACC (red in Figure 8a). Mean summer upwelling velocities w_{Ek} range from 0.2 to 1 m week^{-1} (Figure 8a). Variability is largest over the ACC and over continental shelves (with the exception of the Patagonian shelf off South America, Figure 8b), where maximum w_{Ek}'s are also largest (>1 m week^{-1}, not shown). Summer w_{Ek} can reach 0.8 m d^{-1} or roughly 6 m week^{-1}, which is in the range of values observed in the open ocean [e.g., *Fiechter and Moore*, 2009]. The island effect due to the orographic obstruction of winds shows as a dipole in w_{Ek} over major islands,

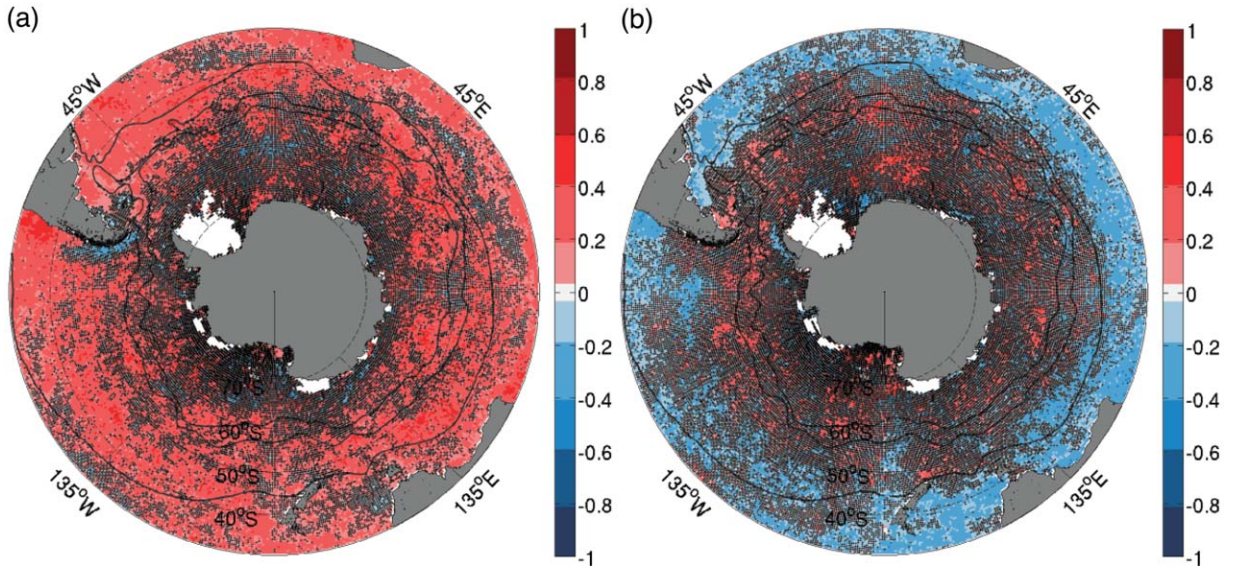

Figure 7. Local summer (DJF) correlation coefficients between high-pass filtered daily anomalies of (a) Chl-a and wind speed and (b) Chl-a and Q_{net}, considering spatial scales larger than 350 km and time scales of less than 10 days that highlight the effect of atmospheric storms. Dotted areas indicate the correlation is not significant to the 90% level. The mean positions of the STF, SAF and PF are shown in black contours.

e.g., in Tasmania, New Zealand, South Georgia, and Kerguelen, with upwelling to the north and downwelling to the south.

Surface wind direction and the wind stress curl can be significantly modified over midlatitude SST fronts, and this in turn can influence ocean Ekman pumping at eddy scales [*O'Neill and Chelton*, 2003, 2010]. Here we are interested in the large-scale Ekman pumping effect associated with atmospheric storms, and therefore we retain large spatial scales and short time scales (>350 km × 350 km and <10 days, see section 2.4) when computing correlations with w_{Ek} (Figure 9).

Ekman upwelling brings cold SSTs to the surface over a circumpolar band (blue areas in Figure 9a). The SST response to Ekman-induced upwelling is not restricted to the south of the mean maximum westerlies but is instead shifted northward presumably due to oscillations in the position of the maximum westerlies. However, the correlation between w_{Ek} and Chl-a in Figure 9b is mostly nonsignificant and does not mirror the w_{Ek} versus SST correlations in Figure 9a. Ekman upwelling does appear to enhance summer Chl-a in coastal upwelling systems of the oceans' eastern boundaries and to the north of the STF in the western Pacific and Atlantic (Figure 9b). On the whole, Ekman upwelling has less impact on summer Chl-a than wind speed, and its impact is localized.

3.5. SST and Chl-a

Changes in SST provide another index of variability in the upper ocean that can impact phytoplankton [*Behrenfeld et al*., 2006, 2008; *O'Malley et al*., 2010]. In this section, we look separately at the influence of SST on Chl-a, because it shows complex patterns that cannot be solely attributed to shoaling or deepening of the MLD at synoptic scales and are likely influenced by mesoscale processes.

Because SST responds to atmospheric forcing as well as a whole range of upper ocean processes, SST anomalies can only partially indicate subsurface entrainment and changes in MLD (see section 3.2). In Figure 10a, by computing partial correlations while controlling for Q_{net} we are able to interpret SST anomalies more clearly as a signature of an oceanic process. Horizontal processes, however, can obscure the correlation patterns resulting from vertical entrainment, and this is more pronounced at weekly time scales. Although the patterns in Figure 10a remain largely unchanged when using spatially smoothed fields that suppress the effect of advection by the mean currents or oceanic mesoscale features, horizontal (and nonlinear) processes may remain in the time domain at weekly time scales, because these act over longer time scales (i.e., weeks to months).

Summer Chl-a anomalies over the Southern Ocean are strongly correlated with SST anomalies, showing large and statistically significant positive or negative correlations over coherent areas at weekly time scales (Figure 10a). Although the SST may have a direct impact on phytoplankton growth by enhancing metabolic rates

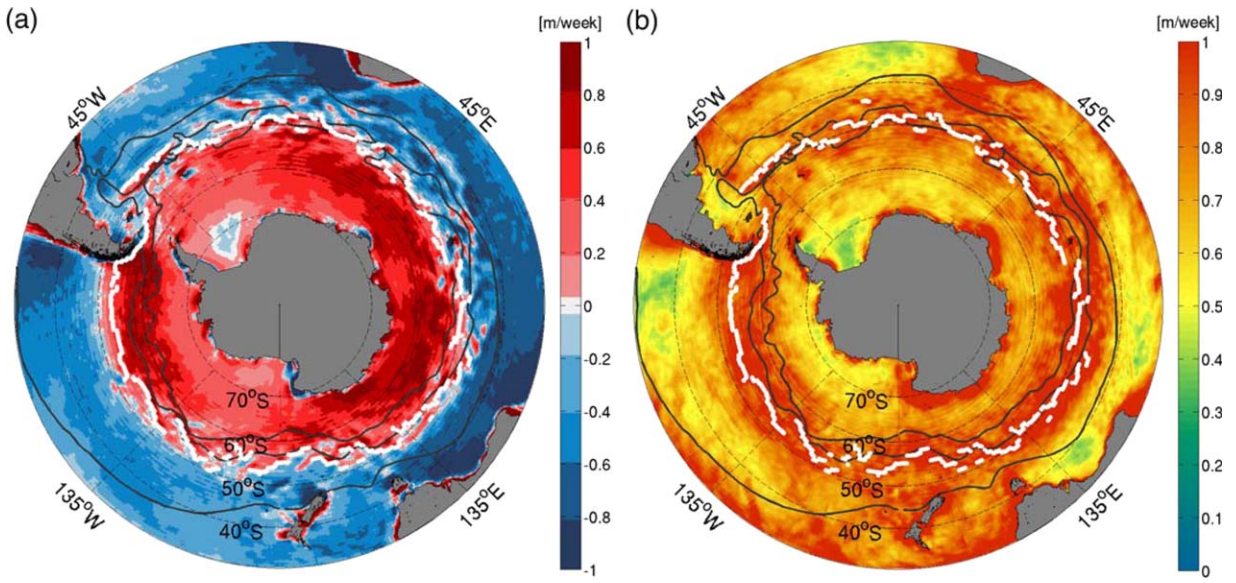

Figure 8. (a) Mean summer (DJF) Ekman pumping velocities (w_{Ek}) in m week^{-1}, based on weekly data for the period 2000–2011. (b) Standard deviation of summer w_{Ek}. The white dotted line indicates the mean position of maximum westerlies. The mean positions of the STF, SAF, and PF are shown in black contours.

[*Eppley*, 1972; *Neori and Holm-Hansen*, 1982; *Reay et al*., 2001], in Figure 10a correlation patterns are tightly linked to frontal features, suggesting oceanic circulation and stratification as main drivers of these correlations, again revealing the close connection between phytoplankton and their physical environment [*O'Malley et al*., 2010].

Regions where Chl-a and SST are inversely related are potential regions where entrainment or upwelling may be at work (e.g., to the north of the STF, to the north of the PF in the eastern Pacific, and between the SAF and PF to the south of Africa). Negative correlations (−0.2 to −0.9) observed mostly to the north of the STF in Figure 10 are consistent with enhanced Chl-a driven by entrainment of cold and presumably nutrient-rich waters from below the euphotic zone due to enhanced wind-mixing (Figure 7a) and surface cooling (Figure 7b), rather than Ekman upwelling (Figure 9a).

When only variability of less than 10 days is considered, SST and Chl-a are uniformly negatively correlated (Figure 10b) and consistent with the entrainment hypothesis. Figure 10b uses high-pass filtered daily anomalies to emphasize the fraction of variance that can be attributed to MLD deepening at the scales of atmospheric storms. Remarkably, positive correlations in Figure 10a vanish and become nonsignificant in Figure 10b. Positive correlations (0.2–0.9) in Figure 10a are observed over most of the Sub-Antarctic Zone (SAZ, the region between the STF and SAF), to the south of the PF in localized regions (e.g., downstream of South Georgia and South Sandwich Islands, and Kerguelen Plateau, or in the central Pacific), and west of the Antarctic Peninsula. Although positive correlations in Figure 10a may imply a shoaling of the MLD and light-limiting conditions, they vanish when considering synoptic time scales (Figure 10b) and are, therefore, likely influenced by oceanic mesoscale processes that operate over longer time scales.

3.6. Discussion

We showed evidence of MLD deepening due to strong winds in the summer over subtropical regions, and most surprisingly, over the ACC where mixed layers are deepest. This is in agreement with recent high-resolution glider observations in the SAZ [*Swart et al*., 2014]. The mechanisms by which winds deepen the mixed layer are beyond the scope of this work, but could include effects of Langmuir circulation [*Kukulka et al*., 2009; *Smith*, 1998; *Li and Garrett*, 1997; *Li et al*., 1995] that is expected to have a significant effect in the Southern Ocean where winds are persistent and the Stokes drift is large [*Belcher et al*., 2012], and/or shear-induced turbulence [*Klein and Coste*, 1984]. Wind gustiness at synoptic time scales can also have an impact on the MLD through wave-induced mixing processes that can potentially facilitate mixing across the base of the seasonal mixed layer [*Babanin et al*., 2009]; however, we find no correlation between wind gustiness and Chl-a (not shown). Wind-induced mixing can input nutrients into the euphotic zone and thus may drive the positive correlations we observe between winds and

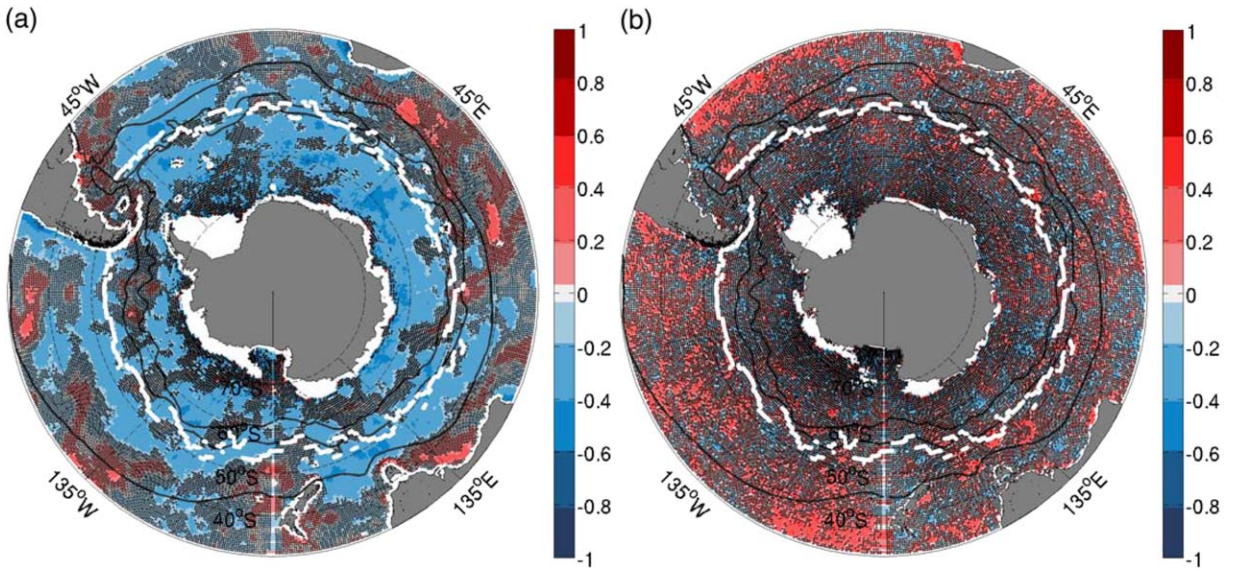

Figure 9. Summer (DJF) partial correlation coefficients, controlling for Q_{net}, between weekly anomalies of (a) w_{Ek} and SST, and (b) w_{Ek} and Chl-a, considering spatial scales larger than 350 km × 350 km and time scales of less than 10 days that highlight the effect of atmospheric storms. Dotted areas indicate that the correlation is not significant to the 90% level. The white dotted line indicates the mean position of maximum westerlies. The mean positions of the STF, SAF, and PF are shown in black contours.

Chl-a over most of the Southern Ocean (Figure 7a). This is in agreement with *Fauchereau et al.* [2011], who based their analysis on satellite observations, ocean reanalysis and a biogeochemical model. They found that Southern Ocean summer Chl-a variability responds to subseasonal changes in the MLD by modulating light and nutrient limitation.

The influence of wind-driven entrainment on Chl-a is associated with atmospheric synoptic storms. This is suggested by correlations based on filtered anomalies that highlight the variability on the scales of the storms (i.e., time scales of $<$10 days and spatial scales $>$350 km, in Figure 7). The combined analysis of correlation patterns based on significant partial correlations of filtered data, controlling for Q_{net}, is summarized in Figure 11. To construct Figure 11, we first plot in light blue regions where blooms are associated with high winds (i.e., red in Figure 7a). Overlaid in green we plot regions where blooms are associated with cold SSTs (i.e., blue in Figure 10b), and

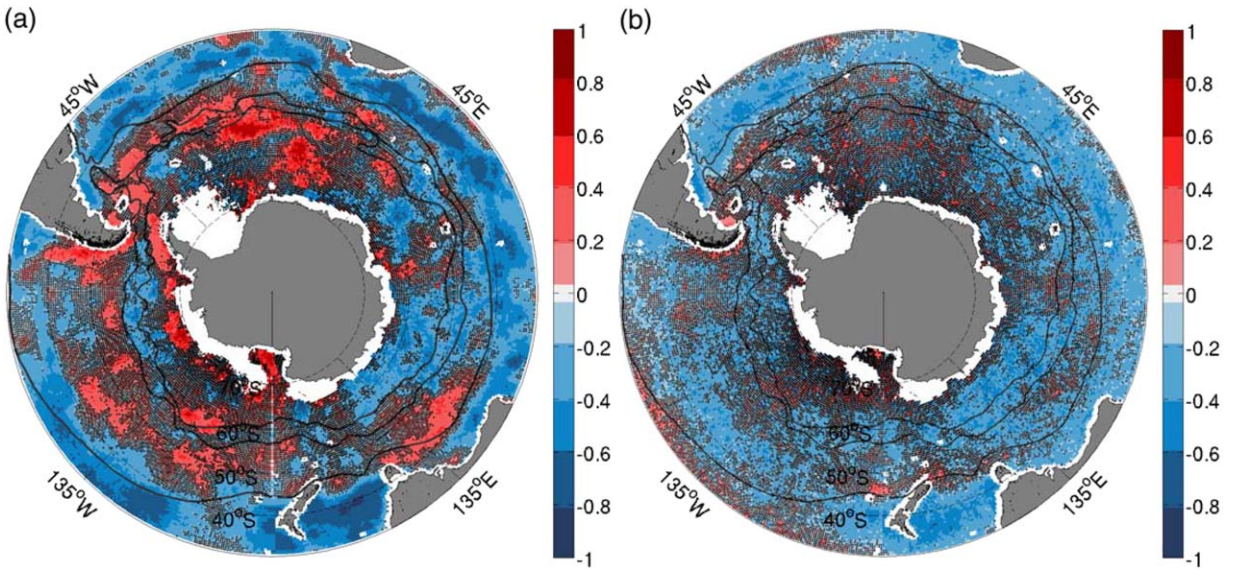

Figure 10. Partial correlation coefficients between (a) weekly anomalies of Chl-a and SST, and (b) high-pass filtered daily anomalies of Chl-a and SST, controlling for the effect of Q_{net}, and considering spatial scales larger than 350 km × 350 km. Dotted areas indicate the correlation is not significant to the 90% level. The mean positions of the STF, SAF, and PF are shown in black contours.

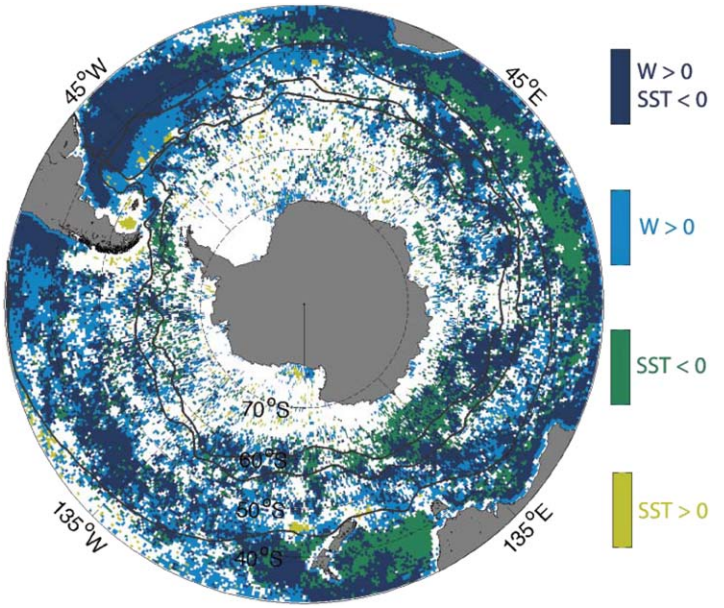

Figure 11. Summary figure showing pixels were positive anomalies of Chl-a are associated with positive anomalies in wind speed (light blue), negative anomalies in SST (dark green), both positive anomalies in wind speed and negative anomalies in SST (blue), and positive anomalies in SST (light green). Regions in blue are consistent with enhanced Chl-a associated with wind-driven entrainment of cold and presumably nutrient-rich waters at synoptic time scales. This map was constructed based on significant partial correlations of spatially smoothed and high-pass filtered data in the time domain (i.e., spatial scales >350 km and time scales <10 days), controlling for Q_{net}.

overlapped regions where both high winds and cold SSTs enhance blooms are indicated in blue. Finally, overlaid in light green we plot regions where blooms are associated with warm SSTs (red in Figure 10b). Therefore, Figure 11 can be interpreted as follows: blue regions indicate blooms that are potentially associated with wind-driven entrainment, regions in light blue are those where blooms are associated with high winds that are not necessarily accompanied by changes in the SST, green regions are those where blooms are associated with cold SSTs presumably caused by processes unrelated to high winds, and in light green regions blooms are associated with warm SSTs that may respond to a shoaling of the MLD, suggesting a light-limited environment.

On shelves, blooms may respond differently to winds than they do in the open ocean. In more quiescent shelf waters under the influence of freshwater input, thin mixed layers can develop (~5 m), and large phytoplankton biomass may result in self-shading leading to more complex interactions between light levels, mixing depth, and nutrient supply [*Vernet et al.*, 2008]. For instance, stratification of shelf waters off the southern tip of South America and in the Marginal Ice Zone (MIZ) that surrounds the Antarctic continent is strongly influenced by freshwater fluxes from glacial origins and sea-ice melting, which stratify the upper ocean but also have the potential to release Fe to surface waters. Blooms in the MIZ have been associated with low winds [*Fitch and Moore*, 2007] and the retreat of the ice shelves and sea-ice melting [e.g., *Arrigo et al.*, 1998; *Vernet et al.*, 2008].

High winds leading to high Chl-a through entrainment of nutrients presumes a biomass increase due to enhanced growth rates. However, phytoplankton biomass accumulation reflected in Chl-a also depends on loss rates that can be caused by grazing. *Behrenfeld*'s [2010] Dilution-Recoupling Hypothesis provides an alternate mechanism to explain the links between the deepening of the mixed layer and increases in Chl-a. In this view, net phytoplankton growth results from a delicate balance between phytoplankton specific growth rates and grazing. Physical processes such as vertical mixing can also modulate grazing rates and alter the balance by dilution: as the MLD deepens, phytoplankton-free waters are entrained into the mixed layer, lowering both prey-predator encounter rates and grazing pressure on phytoplankton [*Marra and Barber*, 2005; *Behrenfeld*, 2010]. The dilution process presumes no subsurface Chl-a maximum, and therefore requires that the MLD exceed the euphotic depth which is more likely to be the case in ACC waters than in subtropical waters.

To our knowledge, the direct relationship between SST and Chl-a in the SAZ in Figure 10a has not been previously documented from satellite measurements. The positive correlations between SST and Chl-a that we observe in the SAZ might suggest that a warm shallow mixed layer promotes high Chl-a, which would imply that relatively deep summer MLDs in the SAZ lead to light limitation. However, such shoaling of the MLD cannot be attributed to reduced wind-mixing or surface warming at synoptic time scales. High-pass filtered data in the time domain (Figure 10b) suggest mesoscale processes cannot be ruled out in Figure 10a and may also be responsible for positive correlations between Chl-a and SST.

Mesoscale eddies and fronts that are ubiquitous in the Southern Ocean can modify upper ocean stratification and SST. Particularly, during times of weak air-sea fluxes or in the presence of strong horizontal gradients,

horizontal dynamics can play a leading order role in restratifying the mixed layer [*Lapeyre et al*., 2006; *Fox-Kemper et al*., 2008]. Close to frontal regions, the stratification of the surface mixed layer is set by the competing effects of ageostrophic circulation, baroclinic instabilities, and eddies, which tend to restratify the upper ocean, and turbulent mixing (i.e., driven by winds and buoyancy forcing) which destroys stratification [*Lapeyre et al*., 2006; *Taylor and Ferrari*, 2011b]. Numerical simulations and observations show that restratification at fronts inhibits vertical mixing, and can trigger phytoplankton blooms in low-light conditions, even in the presence of strong surface cooling and destabilizing winds [*Taylor and Ferrari*, 2011b; *D'Asaro et al*., 2011], as well as eddy-driven stratification [*Mahadevan et al*., 2012].

In the SAZ, the positive correlations between SST and Chl-a suggest that weak background stratification may precondition waters to permit formation of deep mixed layers, and intense mesoscale dynamics assist in the restratification of the surface layer triggering phytoplankton blooms. This scenario is in agreement with biogeochemical modeling and observations in the SAZ south of Africa [*Llido et al*., 2005; *Swart et al*., 2014]. These studies found a strong influence of sub seasonal MLD variability on bloom occurrence, that may in fact extend to many regions throughout the SAZ. For example, *Llido et al*. [2005] found bloom occurrence was linked to strong stratification and upwelling, either caused by cyclonic eddies or local Ekman pumping. Ekman-induced upwelling results in cold SSTs over the SAZ (blue in Figure 9a) but appears to have little impact on Chl-a (red in Figure 9b) at storm's scales. Anticyclonic eddies, however, generally associated with warm SST anomalies, are in agreement with the joint variability between SST and Chl-a that we observe in the SAZ. Enhanced Chl-a in warm core eddies has been observed [e.g., *Mizobata et al*., 2002; *Waite et al*., 2007; *McGillicuddy et al*., 2007; *Kim et al*., 2011; *Lehahn et al*., 2011], and nonlinear mechanisms for nutrient supply and Chl-a enhancement within anticyclonic eddies have been proposed [*Martin and Richards*, 2001; *Mahadevan et al*., 2008], as well as the advection of warm high-chlorophyll waters by anticyclones [*Lehahn et al*., 2011].

Another plausible physical explanation for positive correlations between SST and Chl-a is linked to the meandering and eastward advection of waters in the ACC [*Meskhidze et al*., 2007]. Upwelling and downwelling motions were observed in the meandering of the PF [*Strass et al*., 2002]. An ocean-plankton model suggests that due to the fast surface currents of the ACC, enhanced Chl-a can occasionally occur in downwelling areas, and low Chl-a can occur in upwelling areas [*Hense et al*., 2003]. This is because newly upwelled water near the surface has low Chl-a, but it is rich in nutrients and therefore can sustain phytoplankton growth while it is advected, and until a downwelling event occurs.

Wind-driven Ekman currents are another factor that can supply nutrients and restratify or destratify the mixed layer in cases when the wind stress has a component directed along the front [*Thomas and Ferrari*, 2008; *D'Asaro et al*., 2011]. When the wind is oriented down front, as is most likely the case over the ACC fronts, northward Ekman transport carries waters from the cold side of the front to the warm side which tends to destabilize the water column to the north, driving convective mixing and a reduction of stratification. In the SAZ, one suggestion is that micronutrients are supplied by northward Ekman transport of nutrient-rich waters from the Polar Frontal Zone (PFZ, the region between the PF and SAF) [e.g., *Pollard et al*., 2002]. Such Ekman transport would carry cold SSTs from the south. Therefore, under the assumption that nutrients limit summertime growth, upwelling or mixing and the horizontal advection of nutrients from the south would all imply negative correlations between Chl-a and SST, but we showed this is not the case in the SAZ (see red in Figure 10a). In the PFZ, however, the negative correlations between SST and Chl-a (Figure 10a) could be consistent with a destabilizing effect of Ekman advection. This perhaps suggests a preconditioning of stratification imposed by frontal dynamics and nutrient-limited conditions to the north of the PF that is alleviated during periods of Ekman advection of cold and nutrient-rich waters from the south.

4. Summary and Conclusions

In this study, we have explored the influence of the atmospheric forcing on upper ocean processes (i.e., MLD deepening and Ekman-induced upwelling) that can influence summer Chl-a variability in the Southern Ocean. Recognizing the limitations of a correlation analysis, which does not allow for the determination of causality, we analyze correlation patterns between Chl-a and physical variables, focusing mainly on the potential of nutrient entrainment through the base of the seasonal mixed layer, although other possible mechanisms have also been discussed.

On daily to weekly time scales, summer Chl-a is more influenced by wind-induced entrainment through MLD deepening than by Ekman-induced upwelling. The wind stress curl, which drives Ekman pumping, showed weak

correlations with Chl-a. Ekman pumping, subject to horizontal convergences and divergences, may be more influential on longer time scales [*de Szoeke*, 1980; *Fiechter and Moore*, 2009], and/or on regional and eddy scales.

Wind speed and Chl-a show significant correlations over large areas in the Southern Ocean, confirming that strong winds measurably influence phytoplankton blooms [*Kahru et al*., 2010]. However, in contrast with *Kahru et al*. [2010] who used year-round data, we find strong winds enhance Chl-a in the summer suggesting wind-driven entrainment helps sustain phytoplankton blooms.

The impact of wind-driven entrainment on Chl-a is broader on daily time scales, and it is associated with atmospheric synoptic storm scales. More surprisingly, positive correlations between wind speed and Chl-a are found even over regions with deep summer mixed layers, suggesting that anomalous winds have the potential to deepen the mixed layer, entraining subsurface waters into the euphotic zone effectively without completely eroding the seasonal mixed layer. Using rates of change of MLD from Argo floats, *Tagliabue et al*. [2014] find negligible Fe entrainment fluxes from transient MLD deepening. Our results based on high-resolution satellite data suggest transient MLD deepening may entrain additional Fe on shorter time scales than those resolved by Argo floats (i.e., 10 days at most).

With our approach and the available data, however, we cannot address whether the influence of winds on surface Chl-a is through entrainment of nutrients impacting phytoplankton growth rates, entrainment of phytoplankton-rich waters from a subsurface Chl-a maximum or reduced grazing pressure on phytoplankton. The underlying process can have profound implications on the biological pump, and the acquisition of subsurface Chl-a and nutrient data in the Southern Ocean would be beneficial to help shed light on these. A better understanding of Southern Ocean biology and biogeochemistry is essential regarding projections for the Southern Ocean carbon sink.

As a response to global warming and ozone depletion, Southern Hemisphere westerlies have intensified and shifted southward predominantly in the summer [*Thompson et al*., 2011]. This study suggests that phytoplankton biomass could increase in response to higher summer winds, with potential atmospheric CO_2 drawdown and subsequent enhancement of the biological pump [*Marinov et al*., 2008], counteracting the outgassing of carbon through enhanced upwelling of deep waters that are rich in dissolved inorganic carbon [*Russell et al*., 2006]. Moreover, given that stratification is expected to increase in a changing climate [e.g., *Capotondi et al*., 2012], the importance of wind-driven entrainment might increase more than linearly in the future.

Acknowledgments

We thank the data processing workgroups from JPL, GlobColour, RSS, NCEP, and the Argo program for providing the data and James Holte for the MLD estimates from Argo. Microwave OI SST data are produced by Remote Sensing Systems and sponsored by National Oceanographic Partnership Program (NOPP), the NASA Earth Science Physical Oceanography Program, and the NASA MEaSUREs DISCOVER Project. Data are available at www.remss.com. NASAs Research, Education and Applications Solution Network (REASoN) and MEaSURES programs funded development of the CCMP wind fields, which are distributed by the Physical Oceanography Distributed Active Archive Center (http://podaac.jpl.nasa.gov/). Chl-a data are processed and distributed by ACRI-ST GlobColour service (http://hermes.acri.fr), supported by EU FP7 MyOcean ESA GlobColour Projects, using ESA ENVISAT MERIS data, NASA MODIS, and SeaWiFS data. Heat fluxes from the CFSR reanalysis are available at http://rda.ucar.edu. The Research Data Archive is managed by the Data Support Section of the Computational and Information Systems Laboratory at the National Center for Atmospheric Research in Boulder, Colorado. This work was funded by a NASA NESFF fellowship (NNX12AN41H 001), the NASA Physical Oceanography Program (NNX08AI82G), NSF grants (ARRA OCE0850350 and ANT-0948338) and the Southern Ocean Carbon and Climate Observations and Modeling (SOCCOM) Project (NSF PLR-1425989). We thank Lynne Talley, Peter Franks and the reviewers for a careful reading and suggestions to improve this manuscript, and Alberto Piola and Rob Pinkel for useful discussions.

References

Alexander, M., A. Capotondi, A. Miller, F. Chai, R. Brodeur, and C. Deser (2008), Decadal variability in the northeast Pacific in a physical-ecosystem model: Role of mixed layer depth and trophic interactions, *J. Geophys. Res.*, *113*, C02017, doi:10.1029/2007JC004359.

Alexander, M. A., J. D. Scott, and C. Deser (2000), Processes that influence sea surface temperature and ocean mixed layer depth variability in a coupled model, *J. Geophys. Res.*, *105*(C7), 16,823–16,842.

Allison, D. B., D. Stramski, and B. G. Mitchell (2010), Seasonal and interannual variability of particulate organic carbon within the Southern Ocean from satellite ocean color observations, *J. Geophys. Res.*, *115*, C06002, doi:10.1029/2009JC005347.

Arrigo, K. R., A. Weiss, and W. Smith Jr. (1998), Physical forcing of phytoplankton dynamics in the southwestern Ross Sea, *J. Geophys. Res.*, *103*(C1), 1007–1021.

Arrigo, K. R., G. L. Van Dijken, and S. Bushinsky (2008), Primary production in the Southern Ocean, 1997–2006, *J. Geophys. Res.*, *113*, C08004, doi:10.1029/2007JC004551.

Atlas, R., R. N. Hoffman, J. Ardizzone, S. M. Leidner, J. C. Jusem, D. K. Smith, and D. Gombos (2011), A cross-calibrated, multiplatform ocean surface wind velocity product for meteorological and oceanographic applications, *Bull. Am. Meteorol. Soc.*, *92*(2), 157–174.

Babanin, A. V., A. Ganopolski, and W. R. C. Phillips (2009), Wave-induced upper-ocean mixing in a climate model of intermediate complexity, *Ocean Modell.*, *29*(3), 189–197.

Baker, A. R., and P. Croot (2010), Atmospheric and marine controls on aerosol iron solubility in seawater, *Mar. Chem.*, *120*(1), 4–13.

Baldwin, M. P. (2001), Annular modes in global daily surface pressure, *Geophys. Res. Lett.*, *28*(21), 4115–4118.

Behrenfeld, M., E. Boss, D. Siegel and D. Shea (2005), Carbon-based ocean productivity and phytoplankton physiology from space, *Global Biogeochem. Cycles*, *19*, GB1006, doi:10.1029/2004GB002299.

Behrenfeld, M., K. H. Halsey and A. J. Milligan (2008), Evolved physiological responses of phytoplankton to their integrated growth environment, *Philos. Trans. R. Soc. B*, *363*, 2687–2703.

Behrenfeld, M. J. (2010), Abandoning Sverdrup's critical depth hypothesis on phytoplankton blooms, *Ecology*, *91*(4), 977–989.

Behrenfeld, M. J., R. T. O'malley, D. A. Siegel, C. R. Mcclain, J. L. Sarmiento, G. C. Feldman, A. J. Milligan, P. G. Falkowski, R. M. Letelier and E. S. Boss (2006), Climate-driven trends in contemporary ocean productivity, *Nature*, *444*, 752–755.

Belcher, S. E., et al. (2012), A global perspective on Langmuir turbulence in the ocean surface boundary layer, *Geophys. Res. Lett.*, *39*, L18605, doi:10.1029/2012GL052932.

Blain, S., et al. (2007), Effect of natural iron fertilization on carbon sequestration in the Southern Ocean, *Nature*, *446*, 1070–1074.

Bonekamp, H., A. Sterl, and G. J. Komen (1999), Interannual variability in the Southern Ocean from an ocean model forced by European Centre for Medium? Range Weather Forecasts reanalysis fluxes, *J. Geophys. Res.*, *104*(C6), 13,317–13,331.

Box, G. E. P., G. M. Jenkins, and G. C. Reinsel (1994), *Time Series Analysis: Forecasting and Control*, 3rd ed., Englewood Cliffs, Prentice Hall, N. J.

Boyd, P. (2002), Environmental factors controlling phytoplankton processes in the Southern Ocean, *J. Phycol.*, *38*, 844–861.

Boyd, P. W., and M. J. Ellwood (2010), The biogeochemical cycle of iron in the ocean, *Nature*, *3*, 675–682, doi:10.1038/ngeo964.

Boyd, P. W., E. Ibisanmi, S. G. Sander, K. A. Hunter, and G. A. Jackson (2010), Remineralization of upper ocean particles: Implications for iron biogeochemistry, *Limnol. Oceanogr. Methods*, *55*(3), 1271–1288.

Campbell, J. (1995), The lognormal distribution as a model for bio-optical variability in the sea, *J. Geophys. Res.*, *100*(C7), 13,237–13,254.

Capotondi, A., M. A. Alexander, N. A. Bond, E. N. Curchitser, and J. D. Scott (2012), Enhanced upper ocean stratification with climate change in the CMIP3 models, *J. Geophys. Res.*, *117*, C04031, doi:10.1029/2011JC007409.

Chisholm, S. W. (2000), Oceanography: Stirring times in the Southern Ocean, *Nature*, *407*, 685–687.

Chiswell, S. (2011), Annual cycles and spring blooms in phytoplankton: Don't abandon Sverdrup completely, *Mar. Ecol. Prog. Ser.*, *443*, 39–50.

Close, S. E., and H. Goosse (2013), Entrainment-driven modulation of Southern Ocean mixed layer properties and sea ice variability in CMIP5 models, *J. Geophys. Res. Oceans*, *118*, 2811–2827, doi:10.1002/jgrc.20226.

D'Asaro, E., C. Lee, L. Rainville, R. Harcourt, and L. Thomas (2011), Enhanced turbulence and energy dissipation at ocean fronts, *Science*, *332*, 318–322.

de Baar, H. J., J. T. De Jong, D. C. Bakker, B. M. Löscher, C. Veth, U. Bathmann, and V. Smetacek (1995), Importance of iron for plankton blooms and carbon dioxide drawdown in the Southern Ocean, *Nature*, *373*, 412–415.

de Baar, H. J. W., et al. (2005), Synthesis of iron fertilization experiments: From the iron age in the age of enlightenment, *J. Geophys. Res.*, *110*, C09S16, doi:10.1029/2004JC002601.

de Boyer Montégut, C., G. Madec, A. S. Fischer, A. Lazar, and D. Iudicone (2004), Mixed layer depth over the global ocean: An examination of profile data and a profile-based climatology, *J. Geophys. Res.*, *109*, C12003, doi:10.1029/2004JC002378.

de Szoeke, R. A. (1980), On the effects of horizontal variability of wind stress on the dynamics of the ocean mixed layer, *J. Phys. Oceanogr.*, *10*, 1439–1454.

Doney, S. C. (2003), Mesoscale variability of Sea-viewing Wide Field-of-view Sensor (SeaWiFS) satellite ocean color: Global patterns and spatial scales, *J. Geophys. Res.*, *108*(C2), 3024, doi:10.1029/2001JC000843.

Dong, S., S. T. Gille, J. Sprintall, and C. Gentemann (2006), Validation of the Advanced Microwave Scanning Radiometer for the Earth Observing System (AMSR-E) sea surface temperature in the Southern Ocean, *J. Geophys. Res.*, *111*, C04002, doi:10.1029/2005JC002934.

Dong, S., J. Sprintall, S. T. Gille, and L. Talley (2008), Southern Ocean mixed-layer depth from Argo float profiles, *J. Geophys. Res.*, *113*, C06013, doi:10.1029/2006JC004051.

Eppley, R. (1972), Temperature and phytoplankton growth in the sea, *Fish. Bull*, *70*(4), 1063–1085.

Eppley, R., and E. Renger (1988), Nanomolar increase in surface layer nitrate concentration following a small wind event, *Deep Sea Res., Part A*, *35*(7), 1119–1125.

Fauchereau, N., A. Tagliabue, L. Bopp, and P. M. S. Monteiro (2011), The response of phytoplankton biomass to transient mixing events in the Southern Ocean, *Geophys. Res. Lett.*, *38*, L17601, doi:10.1029/2011GL048498.

Fennel, K., M. R. Abbott, Y. Spitz, J. Richman, and D. Nelson (2003), Impacts of iron control on phytoplankton production in the modern and glacial Southern Ocean, *Deep Sea Res., Part II*, 50, 833–851.

Fiechter, J., and A. M. Moore (2009), Interannual spring bloom variability and Ekman pumping in the coastal Gulf of Alaska, *J. Geophys. Res.*, *114*, C06004, doi:10.1029/2008JC005140.

Fitch, D. T., and J. K. Moore (2007), Wind speed influence on phytoplankton bloom dynamics in the Southern Ocean Marginal Ice Zone, *J. Geophys. Res.*, *112*, C08006, doi:10.1029/2006JC004061.

Fox-Kemper, B., R. Ferrari, and R. Hallberg (2008), Parameterization of mixed layer eddies. Part I: Theory and diagnosis, *J. Phys. Oceanogr.*, *38*(6), 1145–1165.

Frants, M., S. T. Gille, M. Hatta, W. T. Hiscock, M. Kahru, C. I. Measures, B. G. Mitchell, and M. Zhou (2013), Analysis of horizontal and vertical processes contributing to natural iron supply in the mixed layer in southern Drake Passage, *Deep Sea Res., Part II*, *90*, 68–76.

Gibbons, J. D. (1985), *Nonparametric Statistical Inference*, 2nd ed., Marcel Dekker, N. Y.

Gille, S. T. (2005), Statistical characterization of zonal and meridional ocean wind stress, *J. Atmos. Oceanic Technol.*, *22*(9), 1353–1372.

Guinet, C., X. Xing, E. Walker, and P. Monestiez (2013), Calibration procedures and first dataset of Southern Ocean chlorophyll a profiles collected by elephant seals equipped with a newly developed CTD-fluorescence tags, *Earth Syst. Sci. Data*, *5*, 15–29.

Hense, I., R. Timmermann, A. Beckmann, and U. Bathmann (2003), Regional ecosystem dynamics in the ACC: Simulations with a three-dimensional ocean-plankton model, *J. Mar. Syst.*, *42*(1–2), 31–51.

Henson, S. A., and A. C. Thomas (2007), Interannual variability in timing of bloom initiation in the California Current System, *J. Geophys. Res.*, *112*, C08007, doi:10.1029/2006JC003960.

Hoffmann, L. J., I. Peeken, and K. Lochte (2008), Iron, silicate, and light co-limitation of three Southern Ocean diatom species, *Polar Biol.*, *31*(9), 1067–1080.

Holm-Hansen, O., M. Kahru, and C. D. Hewes (2005), Deep chlorophyll a maxima (DCMs) in pelagic Antarctic waters. II. Relation to bathymetric features and dissolved iron concentrations, *Mar. Ecol. Prog. Ser.*, *297*, 71–81.

Holte, J., and L. Talley (2009), A new algorithm for finding mixed layer depths with applications to Argo data and Subantarctic mode water formation, *J. Atmos. Oceanic Technol.*, *26*(9), 1920–1939.

Holte, J., J. Gilson, L. Talley, and D. Roemmich (2010), Argo Mixed Layers, Scripps Institution of Oceanography/UCSD. [Available at http://mixedlayer.ucsd.edu.]

Hoskins, B., and K. I. Hodges (2005), A new perspective on Southern Hemisphere storm tracks, *J. Clim.*, *18*, 4108–4129.

IOCCG (2004), *Guide to the Creation and Use of Ocean-Colour, Level-3, Binned Data Products, Reports of the International Ocean Colour Coordinating Group*, vol. 4, Dartmouth, Nova Scotia, Canada.

Jickells, T. D. (2005), Global iron connections between desert dust, ocean biogeochemistry, and climate, *Science*, *308*, 67–71.

Kahru, M., and B. G. Mitchell (2010), Blending of ocean colour algorithms applied to the Southern Ocean, *Remote Sens. Lett.*, *1*(2), 119–124.

Kahru, M., S. T. Gille, R. Murtugudde, P. G. Strutton, M. Manzano-Sarabia, H. Wang, and B. G. Mitchell (2010), Global correlations between winds and ocean chlorophyll, *J. Geophys. Res.*, *115*, C12040, doi:10.1029/2010JC006500.

Kim, D., E. J. Yang, K. H. Kim, C. W. Shin, J. Park, S. Yoo, and J. H. Hyun (2011), Impact of an anticyclonic eddy on the summer nutrient and chlorophyll a distributions in the Ulleung Basin, East Sea (Japan Sea), *ICES J. Mar. Sci.*, *69*(1), 23–29.

Klein, P., and B. Coste (1984), Effects of wind-stress variability on nutrient transport into the mixed layer, *Deep Sea Res.*, *31*(1), 21–37.

Knox, G. A. (2007), *Biology of the Southern Ocean*, 2nd ed., 116 pp., CRC Press/Taylor & Francis, Boca Raton, Fla.

Korb, R., M. Whitehouse, A. Atkinson, and S. Thorpe (2008), Magnitude and maintenance of the phytoplankton bloom at South Georgia: A naturally iron-replete environment, *Mar. Ecol. Prog. Ser.*, *368*, 75–91.

Krauss, W., R. Döscher, A. Lehmann, and T. Viehoff (1990), On eddy scales in the eastern and northern North Atlantic Ocean as a function of latitude, *J. Geophys. Res.*, *95*(C10), 18,049–18,056.

Kukulka, T., A. J. Plueddemann, J. H. Trowbridge, and P. P. Sullivan (2009), Significance of Langmuir circulation in upper ocean mixing: Comparison of observations and simulations, *Geophys. Res. Lett.*, *36*, L10603, doi:10.1029/2009GL037620.
Lancelot, C., A. de Montety, H. Goosse, S. Becquevort, V. Schoemann, B. Pasquer, and M. Vancoppenolle (2009), Spatial distribution of the iron supply to phytoplankton in the Southern Ocean: A model study, *Biogeosciences*, *6*(12), 2861–2878.
Lapeyre, G., P. Klein, and B. Hua (2006), Oceanic restratification forced by surface frontogenesis, *J. Phys. Oceanogr.*, *36*(8), 1577–1590.
Le Quéré, C., L. Bopp, and I. Tegen (2002), Antarctic circumpolar wave impact on marine biology: A natural laboratory for climate change study, *Geophys. Res. Lett.*, *29*(10), 1407, doi:10.1029/2001GL014585.
Lee, T., O. Wang, W. Tang, and W. T. Liu (2008), Wind stress measurements from the QuikSCAT-SeaWinds scatterometer tandem mission and the impact on an ocean model, *J. Geophys. Res.*, *113*, C12019, doi:10.1029/2008JC004855.
Lehahn, Y., F. d'Ovidio, M. Lévy, Y. Amitai, and E. Heifetz (2011), Long range transport of a quasi isolated chlorophyll patch by an Agulhas ring, *Geophys. Res. Lett.*, *38*, L16610, doi:10.1029/2011GL048588.
Lévy, M., P. Klein, and M. Ben Jelloul (2009), New production stimulated by high-frequency winds in a turbulent mesoscale eddy field, *Geophys. Res. Lett.*, *36*, L16603, doi:10.1029/2009GL039490.
Li, M., and C. Garrett (1997), Mixed layer deepening due to Langmuir circulation, *J. Phys. Oceanogr.*, *27*, 121–132.
Li, M., K. Zahariev, and C. Garrett (1995), Role of Langmuir circulation in the deepening of the ocean surface mixed layer, *Science*, *270*, 1955–1957.
Llido, J., V. Garçon, J. Lutjeharms, and J. Sudre (2005), Event-scale blooms drive enhanced primary productivity at the Subtropical Convergence, *Geophys. Res. Lett.*, *32*, L15611, doi:10.1029/2005GL022880.
Lovenduski, N. S., and N. Gruber (2005), Impact of the southern annular mode on Southern Ocean circulation and biology, *Geophys. Res. Lett.*, *32*, L11603, doi:10.1029/2005GL022727.
Luo, C., N. Mahowald, and N. Meskhidze (2005), Estimation of iron solubility from observations and a global aerosol model, *J. Geophys. Res.*, *110*, D23307, doi:10.1029/2005JD006059.
Mahadevan, A., E. D'Asaro, C. Lee, and M. J. Perry (2012), Eddy-Driven Stratification Initiates North Atlantic Spring Phytoplankton Blooms, *Science*, *337*(6090), 54–58, doi:10.1126/science.1218740.
Mahadevan, A., L. N. Thomas, and A. Tandon (2008), Comment on "Eddy/wind interactions stimulate extraordinary mid-ocean plankton blooms", *Science*, *320*, 448.
Marinov, I., M. Follows, A. Gnanadesikan, J. L. Sarmiento, and R. D. Slater (2008), How does ocean biology affect atmospheric pCO_2? Theory and models, *J. Geophys. Res.*, *113*, C07032, doi:10.1029/2007JC004598.
Maritorena, S., and D. Siegel (2005), Consistent merging of satellite ocean color data sets using a bio-optical model, *Remote Sens. Environ.*, *94*, 429–440.
Marra, J., and R. Barber (2005), Primary productivity in the Arabian Sea: A synthesis of JGOFS data, *Prog. Oceanogr.*, *65*, 159–175.
Marra, J., R. Bidigare, and T. Dickey (1990), Nutrients and mixing, chlorophyll and phytoplankton growth, *Deep Sea Res., Part A*, *37*, 127–143.
Martin, A. P., and K. J. Richards (2001), Mechanisms for vertical nutrient transport within a North Atlantic mesoscale eddy, *Deep Sea Res., Part II*, *48*, 757–773.
Martin, J., S. Fitzwater, and R. Gordon (1990a), Iron deficiency limits phytoplankton growth in Antarctic waters, *Global Biogeochem. Cycles*, *4*(1), 5–12.
Martin, J., R. Gordon, and S. Fitzwater (1990b), Iron in Antarctic waters, *Nature*, *345*, 156–158.
Martin, P., et al. (2013), Iron fertilization enhanced net community production but not downward particle flux during the Southern Ocean iron fertilization experiment LOHAFEX, *Global Biogeochem. Cycles*, *27*, 871–881, doi:10.1002/gbc.20077.
McGillicuddy, D. J., et al. (2007), Eddy/wind interactions stimulate extraordinary mid-ocean plankton blooms, *Science*, *316*, 1021–1026.
McPhaden, M. J., M. F. Cronin, and D. C. McClurg (2008), Meridional structure of the seasonally varying mixed layer temperature balance in the eastern tropical Pacific, *J. Clim.*, *21*, 3240–3260.
Meskhidze, N., A. Nenes, W. Chameides, C. Luo, and N. Mahowald (2007), Atlantic Southern Ocean productivity: Fertilization from above or below?, *Global Biogeochem. Cycles*, *21*, GB2006, doi:10.1029/2006GB002711.
Miller, C. B., B. W. Frost, B. Booth, P. A. Wheeler, M. R. Landry, and N. Welschmeyer (1991), Ecological processes in the subarctic Pacific: Iron limitation cannot be the whole story, *Oceanography*, *4*(2), 71–78.
Mitchell, B., and O. Holm-Hansen (1991), Observations of modeling of the Antarctic phytoplankton crop in relation to mixing depth, *Deep Sea Res., Part A*, *38*(8/9), 981–1007.
Mizobata, K., S. Saitoh, A. Shiomoto, T. Miyamura, N. Shiga, K. Imai, M. Toratani, Y. Kajiwara, and K. Sasaoka (2002), Bering Sea cyclonic and anticyclonic eddies observed during summer 2000 and 2001, *Prog. Oceanogr.*, *55*, 65–75.
Moore, J., and M. Abbott (2000), Phytoplankton chlorophyll distributions and primary production in the Southern Ocean, *J. Geophys. Res.*, *105*(C12), 28,709–28,722.
Moore, J. K. (2004), Upper ocean ecosystem dynamics and iron cycling in a global three-dimensional model, *Global Biogeochem. Cycles*, *18*, GB4028, doi:10.1029/2004GB002220.
Musgrave, D., J. Chou, and W. Jenkins (1988), Application of a model of upper-ocean physics for studying seasonal cycles of oxygen, *J. Geophys. Res.*, *93*(C12), 15,679–15,700.
Nakamura, H., T. Izumi, and T. Sampe (2002), Interannual and decadal modulations recently observed in the Pacific storm track activity and East Asian winter monsoon, *J. Clim.*, *15*, 1855–1874.
Neori, A., and O. Holm-Hansen (1982), Effect of temperature on rate of photosynthesis in Antarctic phytoplankton, *Polar Biol.*, *1*, 33–38.
O'Malley, R. T., M. J. Behrenfeld, D. A. Siegel, and S. Maritorena (2010), Global ocean phytoplankton [in *State of the Climate in 2009*, edited by D. S. Arndt, M. O. Baringer, and M. R. Johnson], *Bull. Am. Meteorol. Soc.*, *91*(7), S75–S78.
O'Neill, L., and D. Chelton (2003), Observations of SST-induced perturbations of the wind stress field over the Southern Ocean on seasonal timescales, *J. Clim.*, *16*, 2340–2354.
O'Neill, L., and D. Chelton (2010), The effects of SST-induced surface wind speed and direction gradients on midlatitude surface vorticity and divergence, *J. Clim.*, *23*, 255–281.
Orsi, A., T. Whitworth, and W. Nowlin (1995), On the meridional extent and fronts of the Antarctic Circumpolar Current, *Deep Sea Res., Part I*, *42*(5), 641–673.
Pollard, R., M. Lucas, and J. Read (2002), Physical controls on biogeochemical zonation in the Southern Ocean, *Deep Sea Res., Part II*, *49*, 3289–3305.
Price, J. (1981), Upper ocean response to a hurricane, *J. Phys. Oceanogr*, *11*(2), 153–175.
Racault, M.-F., C. Le Quéré, E. Buitenhuis, S. Sathyendranath, and T. Platt (2012), Phytoplankton phenology in the global ocean, *Ecol. Indicators*, *14*, 152–163.

Reay, D., J. Priddle, D. Nedwell, M. Whitehouse, J. Ellis-Evans, C. Deubert, and D. Connelly (2001), Regulation by low temperature of phytoplankton growth and nutrient uptake in the Southern Ocean, *Mar. Ecol. Prog. Ser.*, *219*, 51–64.
Risien, C., and D. Chelton (2008), A global climatology of surface wind and wind stress fields from eight years of QuikSCAT scatterometer data, *J. Phys. Oceanogr.*, *38*(11), 2379–2413.
Russell, J., K. Dixon, A. Gnanadesikan, R. Stouffer, and J. Toggweiler (2006), The Southern Hemisphere westerlies in a warming world: Propping open the door to the deep ocean, *J. Clim.*, *19*(24), 6382–6390.
Saha, S., et al. (2010a), NCEP Climate Forecast System Reanalysis (CFSR) 6-hourly Products, January 1979 to December 2010, Research Data Archive, Natl. Center for Atmos. Res., Comput. and Inform. Syst. Lab., Boulder, Colo., doi:10.5065/D69K487J.
Saha, S., et al. (2010b), The NCEP climate forecast system reanalysis, *Bull. Am. Meteorol. Soc.*, *91*(8), 1015–1057.
Sallée, J. B., K. G. Speer, and S. R. Rintoul (2010), Zonally asymmetric response of the Southern Ocean mixed-layer depth to the Southern Annular Mode, *Nat. Geosci.*, *3*, 273–279.
Sedwick, P. N., and G. R. Ditullio (1997), Regulation of algal blooms in Antarctic Shelf Waters by the release of iron from melting sea ice, *Geophys. Res. Lett.*, *24*(20), 2515–2518.
Sedwick, P. N., et al. (2011), Early season depletion of dissolved iron in the Ross Sea polynya: Implications for iron dynamics on the Antarctic continental shelf, *J. Geophys. Res.*, *116*, C12019, doi:10.1029/2010JC006553.
Smith, J. (1998), Evolution of Langmuir circulation during a storm, *J. Geophys. Res.*, *103*(C6), 12,649–12,668.
Sokolov, S., and S. R. Rintoul (2007), On the relationship between fronts of the Antarctic Circumpolar Current and surface chlorophyll concentrations in the Southern Ocean, *J. Geophys. Res.*, *112*, C07030, doi:10.1029/2006JC004072.
Stammer, D. (1998), On eddy characteristics, eddy transports, and mean flow properties, *J. Phys. Oceanogr.*, *28*(4), 727–739.
Stephenson, G. R., Jr., S. T. Gille, and J. Sprintall (2012), Seasonal variability of upper ocean heat content in Drake Passage, *J. Geophys. Res.*, *117*, C04019, doi:10.1029/2011JC007772.
Strass, V., A. Naveira Garabato, R. Pollard, H. Fischer, I. Hense, J. Allen, J. Read, H. Leach, and V. Smetacek (2002), Mesoscale frontal dynamics: Shaping the environment of primary production in the Antarctic Circumpolar Current, *Deep Sea Res., Part II*, *49*, 3735–3769.
Sunda, W., and S. Huntsman (1995), Iron uptake and growth limitation in oceanic and coastal phytoplankton, *Mar. Chem.*, *50*, 189–206.
Sverdrup, H. U. (1953), On conditions for the vernal blooming of phytoplankton, *J. Cons. Int. Explor. Mer*, *18*, 287–295.
Swart, S., S. J. Thomalla, and P. M. S. Monteiro (2014), The seasonal cycle of mixed layer dynamics and phytoplankton biomass in the Sub-Antarctic Zone: A high-resolution glider experiment, *J. Mar. Syst.*, doi:10.1016/j.jmarsys.2014.06.002.
Tagliabue, A., J.-B. Sallée, A. R. Bowie, M. Lévy, S. Swart, and P. W. Boyd (2014), Surface-water iron supplies in the Southern Ocean sustained by deep winter mixing, *Nat. Geosci.*, *7*(4), 314–320.
Taylor, J. R., and R. Ferrari (2011a), Shutdown of turbulent convection as a new criterion for the onset of spring phytoplankton blooms, *Limnol. Oceanogr. Methods*, *56*, 2293–2307.
Taylor, J. R., and R. Ferrari (2011b), Ocean fronts trigger high latitude phytoplankton blooms, *Geophys. Res. Lett.*, *38*, L23601, doi:10.1029/2011GL049312.
Thomalla, S. J., N. Fauchereau, S. Swart, and P. M. S. Monteiro (2011), Regional scale characteristics of the seasonal cycle of chlorophyll in the Southern Ocean, *Biogeosciences*, *8*, 2849–2866.
Thomas, L., and R. Ferrari (2008), Friction, frontogenesis, and the stratification of the surface mixed layer, *J. Phys. Oceanogr.*, *38*(11), 2501–2518.
Thompson, D. W. J., S. Solomon, P. J. Kushner, M. H. England, K. M. Grise, and D. J. Karoly (2011), Signatures of the Antarctic ozone hole in Southern Hemisphere surface climate change, *Nat. Geosci.*, *4*, 741–749.
Tréguer, P., and P. Pondaven (2001), Preface: Climatic changes and the carbon cycles in the Southern Ocean: A step forward, *Deep Sea Res., Part II*, *49*, 1597–1600.
Venables, H., and C. M. Moore (2010), Phytoplankton and light limitation in the Southern Ocean: Learning from high-nutrient, high-chlorophyll areas, *J. Geophys. Res.*, *115*, C02015, doi:10.1029/2009JC005361.
Vera, C. (2003), Interannual and interdecadal variability of atmospheric synoptic-scale activity in the Southern Hemisphere, *J. Geophys. Res.*, *108*(C4), 8077, doi:10.1029/2000JC000406.
Verlinden, K. L., D. W. J. Thompson, and G. L. Stephens (2011), The three-dimensional distribution of clouds over the southern hemisphere high latitudes, *J. Clim.*, *24*, 5799–5811.
Vernet, M., D. Martinson, R. Iannuzzi, S. Stammerjohn, W. Kozlowski, K. Sines, R. Smith, and I. Garibotti (2008), Primary production within the sea-ice zone west of the Antarctic Peninsula: I—Sea ice, summer mixed layer, and irradiance, *Deep Sea Res., Part II*, *55*, 2068–2085.
Wagener, T., C. Guieu, R. Losno, S. Bonnet, and N. Mahowald (2008), Revisiting atmospheric dust export to the Southern Hemisphere ocean: Biogeochemical implications, *Global Biogeochem. Cycles*, *22*, GB2006, doi:10.1029/2007GB002984.
Waite, A. M., S. Pesant, D. A. Griffin, P. A. Thompson, and C. M. Holl (2007), Oceanography, primary production and dissolved inorganic nitrogen uptake in two Leeuwin Current eddies, *Deep Sea Res., Part II*, *54*, 981–1002.
Wallace, J. M., T. P. Mitchell, and C. Deser (1989), The influence of sea surface temperature variability on surface wind in the eastern equatorial Pacific: Seasonal and interannual variability, *J. Clim.*, *2*, 1492–1499.
Xie, S.-P. (2004), Satellite observations of cool ocean-atmosphere interaction, *Bull. Am. Meteorol. Soc.*, *85*, 195–208.
Xue, Y., B. Huang, Z.-Z. Hu, A. Kumar, C. Wen, D. Behringer, and S. Nadiga (2011), An assessment of oceanic variability in the NCEP climate forecast system reanalysis, *Clim. Dyn.*, *37*, 2511–2539.
Yuan, X. (2004), High-wind-speed evaluation in the Southern Ocean, *J. Geophys. Res.*, *109*, D13101, doi:10.1029/2003JD004179.